SUPPLEMENTARY INFORMATION

Sub-micron moulding topological mass transport regimes in angled vortex fluidic flow

Thaar M. D. Alharbi, [1,2,9] Matt Jellicoe, [1,9] Xuan Luo, [1,3,9] Kasturi Vimalanathan,[1] Ibrahim K. Alsulami,[1] Bediea S. AL Harbi,[1] Aghil Igder,[1,4] Fayed A. J. Alrashaidi,[1,5] Xianjue Chen,[6] Keith A. Stubbs,[7] Justin M. Chalker,[1] Wei Zhang,[3] Ramiz A. Boulos,[1,8] Darryl B. Jones,[1] Jamie S. Quinton,[1] and Colin L. Raston[*1]*

1. Flinders Institute for Nanoscale Science and Technology, College of Science and Engineering, Flinders University, Bedford Park, SA 5042, Australia colin.raston@flinders.edu.au
2. Physics Department, Faculty of Science, Taibah University, Almadinah Almunawarrah 42353, Saudi Arabia
3. Centre for Marine Bioproducts Development, College of Medicine and Public Health, Flinders University, Adelaide, SA 5042, Australia.
4. School of Engineering, Edith Cowan University, Joondalup, Perth, WA 6027, Australia.
5. Department of Chemistry, College of Science, AlJouf University, Sakaka 72388, Saudi Arabia.
6. School of Chemistry, University of New South Wales, Sydney, NSW 2052, Australia.
7. School of Molecular Sciences, The University of Western Australia, 35 Stirling Hwy, Crawley, WA 6009, Australia.
8. BrightChem Consulting, Suite 16, 45 Delawney Street, Balcatta, WA 6021, Australia.
9. Authors contributed equally to this work

Contents

1. General materials and methods

All chemicals were used as received unless otherwise stated. Fullerene C_{60} (99685-96-8, 99+%) was purchased from BuckyUSA. Graphene oxide (average sheet size: ~ 5 mm in cross section) and high molecular weight polymer beads of polysulfone (PSF) were purchased from Sigma Aldrich. Dichloromethane (DCM) (99.8%), toluene (99.5%) and hexane fraction were purchased from Chem-Supply. Bovine serum albumin (BSA), ethanol, phosphate buffer solution (PBS) and glutaraldehyde were obtained from Sigma-Aldrich as analytical grades. The PBS solution was prepared at 10 mM of pH 7.4 at room temperature using MilliQ water. Zinc acetate dihydrate ($Zn(OAc)_2 \cdot 2H_2O$), terephthalic acid (H_2BDC), dimethylformamide (DMF) and trimethylamine (TEA) were also obtained from Sigma-Aldrich as analytical grades.

Graphene oxide materials, fullerenes materials, macroporous BSA microspheres and metal organic frameworks (MOFs) were characterized using scanning electron microscopy (SEM) performed using a FEI Quanta 450, atomic force microscopy (AFM) using the Nanoscope 8.10 in tapping mode, transmission electron microscopy and high-resolution transmission electron microscopy (TEM and HRTEM) and selected area electron diffraction (SAED), recorded using a JEM- 2100F (200 kV) equipped with an EDS module, and X-ray diffraction data recorded using a Bruker D8 ADVANCE ECO system (Co- Kα, λ=1.7889 Å). Samples for TEM were prepared by drop-casting the material onto standard carbon coated copper grids prior to characterization. Real-time SANS experiments were done at the Australian Nuclear Science and Technology Organisation (ANSTO), using the Quokka instrument.

2. Temperature change in the VFD for different solvents at different rotational speeds (ω) and inclination angle (θ)

A FLIR (T62101) camera was used to record temperature variation of different liquids at rotational speeds between 2k to 9k rpm for the confined mode of operation of the VFD, and 3k to 9k rpm for mimicking the continuous flow mode of operation at an inclination angle θ = 45°. The settings of the FTIR camera included emissivity 0.95, object distance 30.48 cm, relative humidity 50%, and the use of the rainbow colour pallet. All experiments were conducted in triplicate using the same quartz tube for each liquid for consistency of measurements within a temperature-controlled environment (average temperature 19 °C). For the confined mode of operation of the VFD, 1 mL of liquid (unless otherwise stated) was added to the rapidly rotating tube or for mimicking continuous flow processing sufficient liquid was added to the tube such that for any rotational speed, the generated thin film of liquid extends to the lip at the top of the tube.

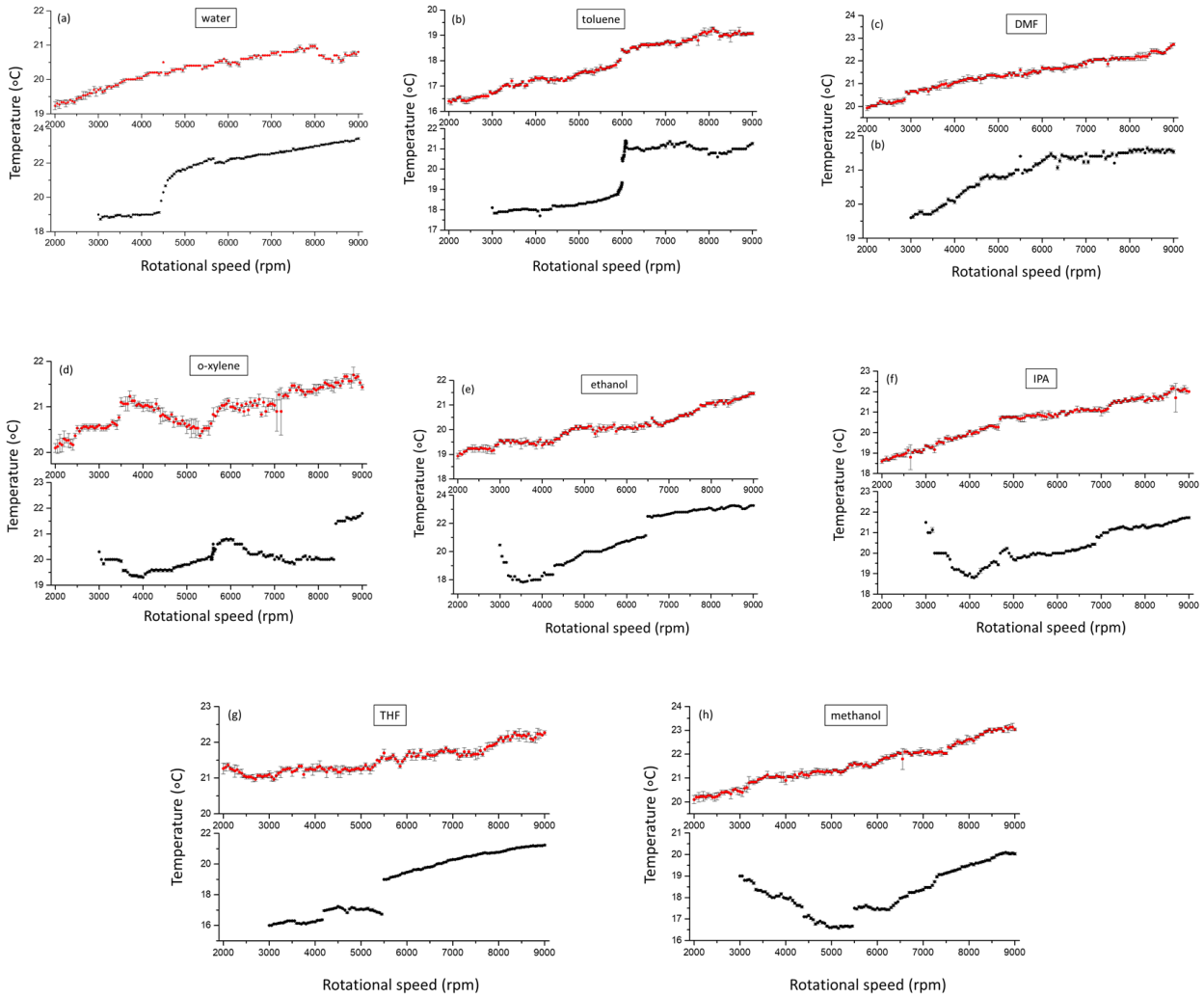

Figure S1: Temperature change of solvents as a function of rotations speed at θ = 45°, ω = 2k to 9k rpm for the confined mode (1mL of liquid (—)) and ω = 3k to 9k rpm for mimicking continuous flow (thin film extended to the lip of the tube, (—)), noting that for the latter, for ω < 3k rpm the vortex in the tube does not expose the bottom of the tube (20 mm OD, 17.5 mm ID).

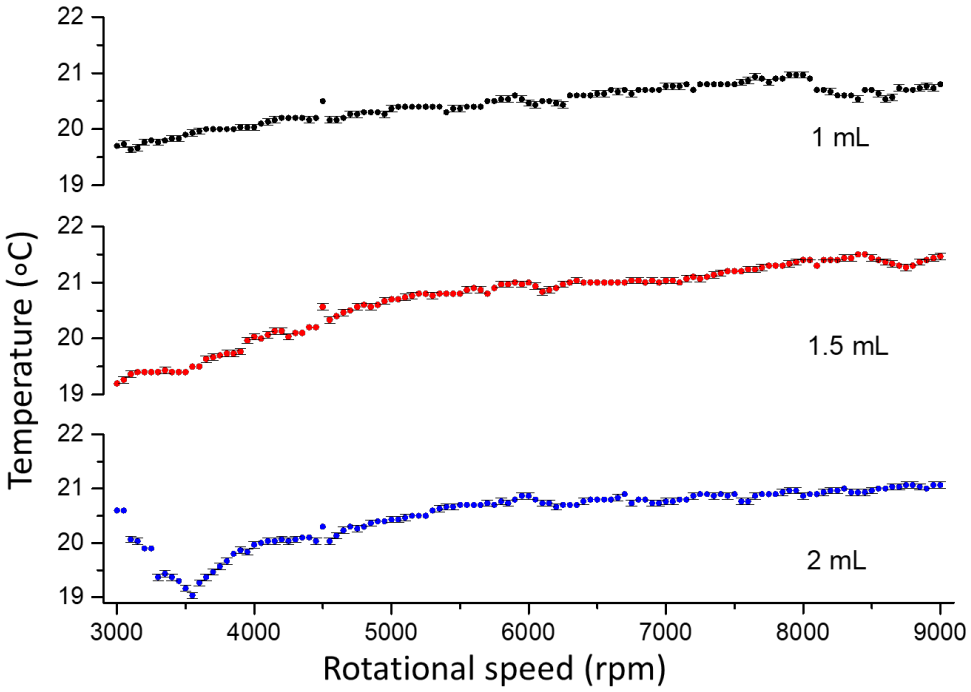

Figure S2: Temperature change as a function of volume of water in a 20 mm OD (17.5 mm ID) rotating tube for the confined mode of operation in the VFD, with θ = 45°.

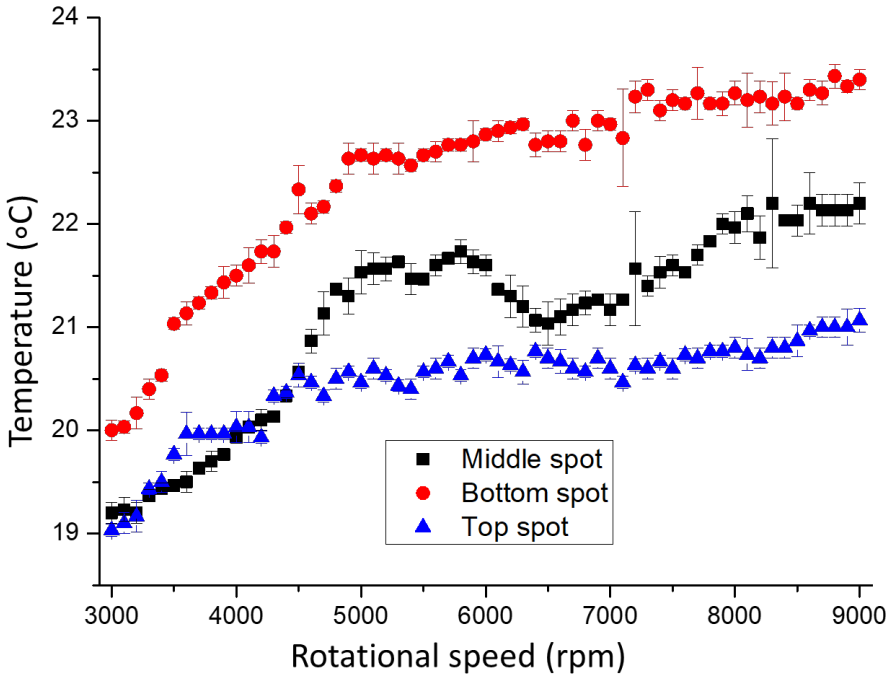

Figure S3: Temperature change for water in a 20 mm OD (17.5 mm ID) tube, 18.5 cm in length, θ = 45°, at 3 different locations on the rotating tube; mid-way along the tube, and 2 cm away from the upper and lower bearings (top and bottom).

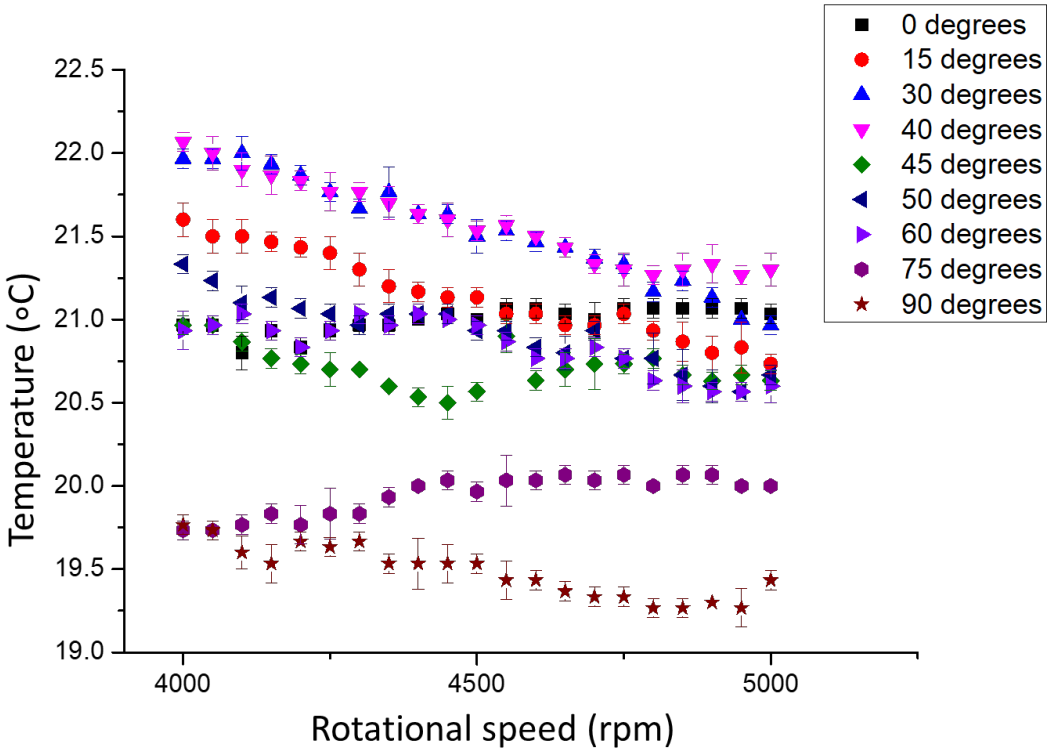

Figure S4: Temperature change measurements for water (mimicking continuous flow) in a 10 mm OD (8.5 mm ID) tube, as a function of change in inclination angle for rotational speeds between 4k and 5k rpm.

3. Mixing times of water at different rotational speeds and inclination angle in a 10 mm OD tube.

Mixing time corresponds to the time taken for a drop of water containing a small amount of dye added at the bottom of the tube rotating at a specific speed to visibly uniformly mix in half way up the preformed film generated from 1 mL of water (measured in triplicates).

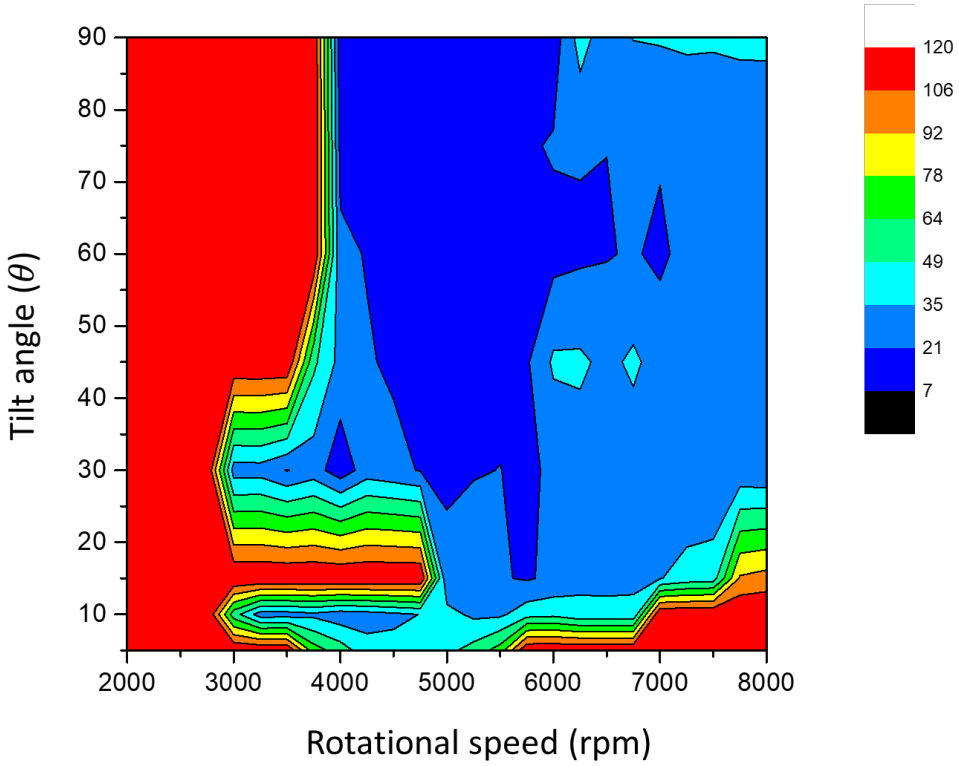

Figure S5: Mixing times (colour pallet in seconds) as a function of ω and θ in a 10 mm OD (8.5 mm ID) tube.

4. Captured images from high speed photography of a thin film in a 10 mm OD VFD glass tube, θ = 45º.

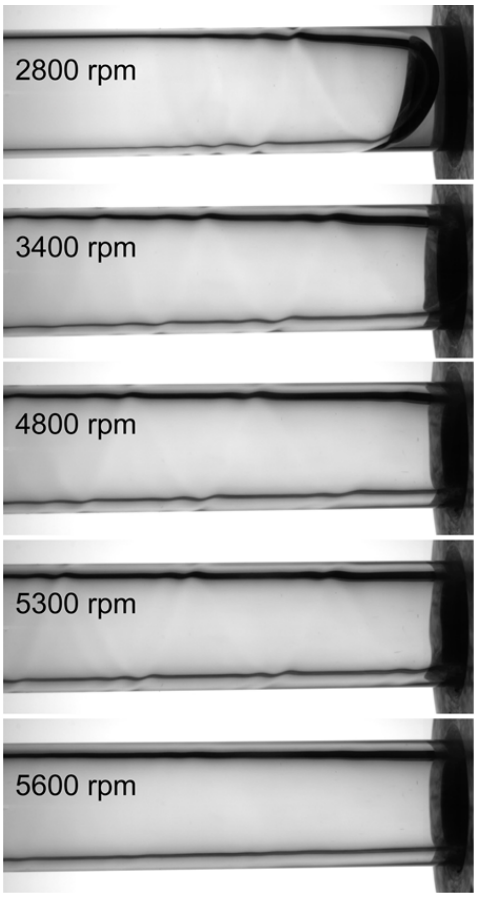

Figure S6: Snapshots were adapted from Video S1 attached. They illustrate the statuses of the liquid (dye water) spun in a 10 mm OD tube (8.5 mm ID) at θ = 45°. The high-speed camera (FASTCAM SA1.1 model 675K-M1) was also positioned at θ = 45°, with a record rate (fps) of 1000. The spinning rates (rotational speeds) were calculated by studying the motion of the tube in each frame with the fps of the video. We noted that circular flow was generated as the tube rotated. The average liquid film thickness decreases with the increase of the spinning rate. There was a sudden transition of the flow (the disappearance of the "wavy" flow) at a rotational rate of ~5.6k rpm, which is close to the value (~6k rpm) recorded in the sudden change in average thickness for a 10 mm tube at θ = 45°, which correspond closely to transitioning from spicule flow to double helical flow.

5. Average film thickness as a function of ω, at θ = 45°.

Excess liquid was added to a weighed quartz tube (20 mm OD, 17.5 mm ID, 18.5 cm in length) and spun at 3k for 1 minute, such that excess liquid was ejected at the top of the tube. After 1 minute the tube was weighed to determine the volume of liquid left post VFD processing. Experiments were repeated for increasing rotational speeds from 3k to 9k rpm at 250 rpm increments, and were all done in triplicates. Water, toluene, DMF, *o*-xylene, DMF/*o*-xylene (1:1 volume ratio) were studied in this way. In addition, water was similarly studied in a 10 mm OD glass tube (8. 5 mm ID). The average film thickness for each liquid was determined according to:

$$d = r - \sqrt{r^2 - \left(\frac{V}{\pi h}\right)}$$

Where d = film thickness (cm) r = radius of tube (cm), V = volume of liquid (mL), and h = height of tube, 18.5 cm.

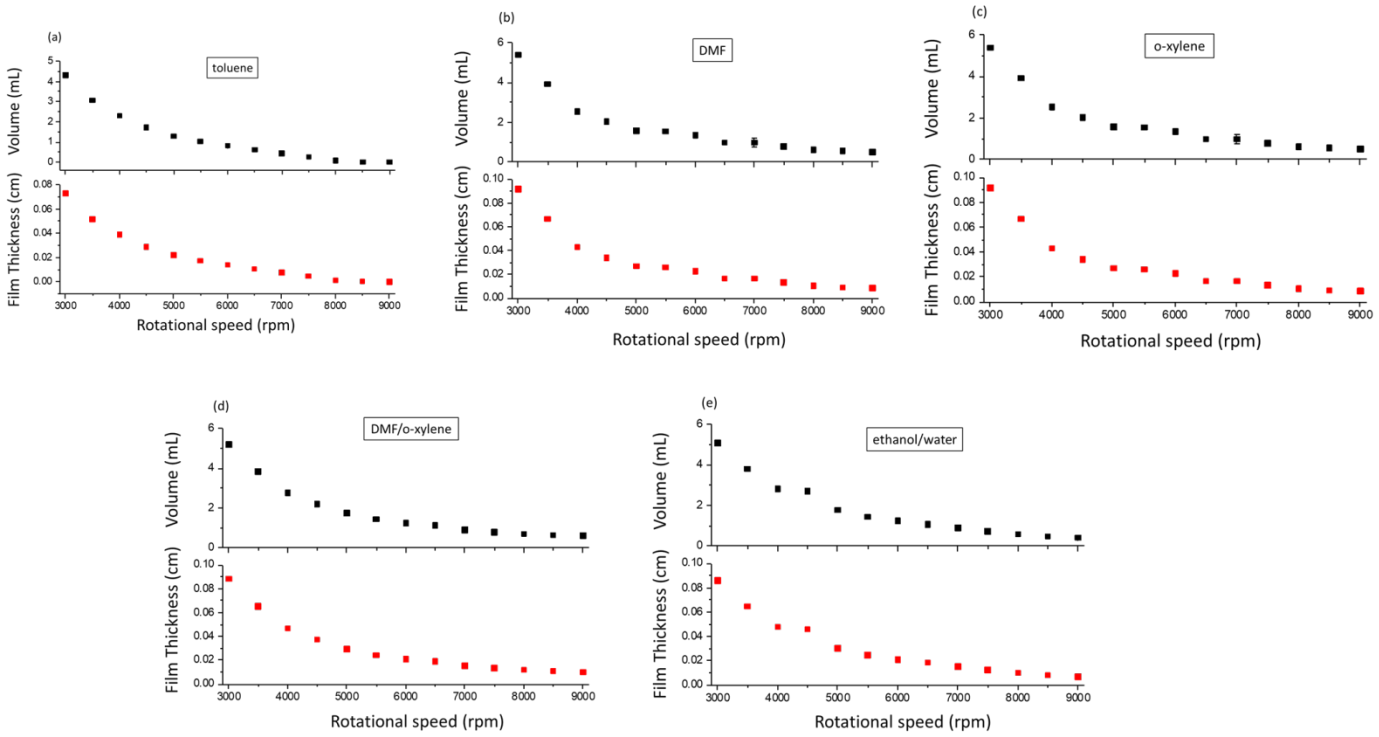

Figure S7: Average film thickness and volume of liquid left in a quartz tube (20 mm OD, 17.5 mm ID, 18.5 cm in length) as a function of ω at θ = 45°, for (a) toluene, (b) DMF, (c) *o*-xylene, (d) DMF/*o*-xylene (1:1 volume ratio) and (e) ethanol/water (1:1 volume ratio).

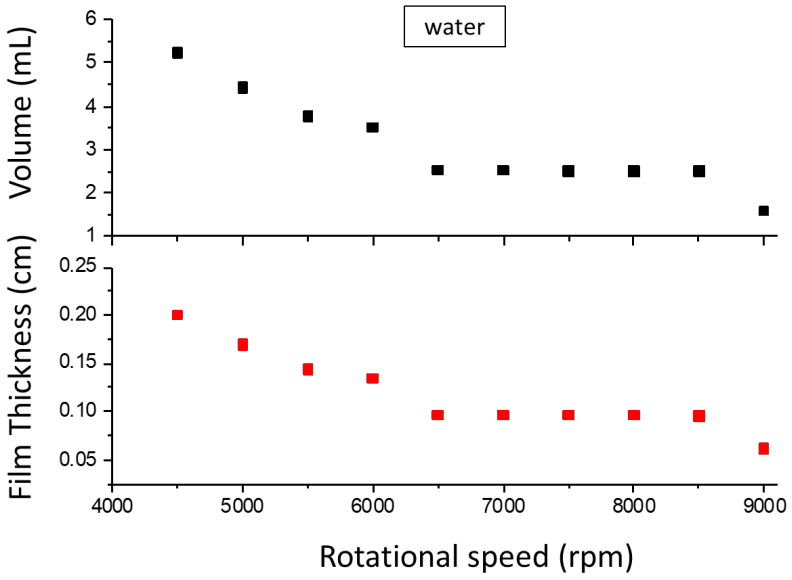

Figure S8: Average film thickness and volume of water left in a quartz tube (10 mm OD, 8.5 mm ID, 18.5 cm in length) as a function of ω at θ = 45°.

6. Manipulating graphene oxide in DMF in the VFD

Outcome of processing of graphene oxide at specific rotational speeds in the VFD, at θ = 45º.

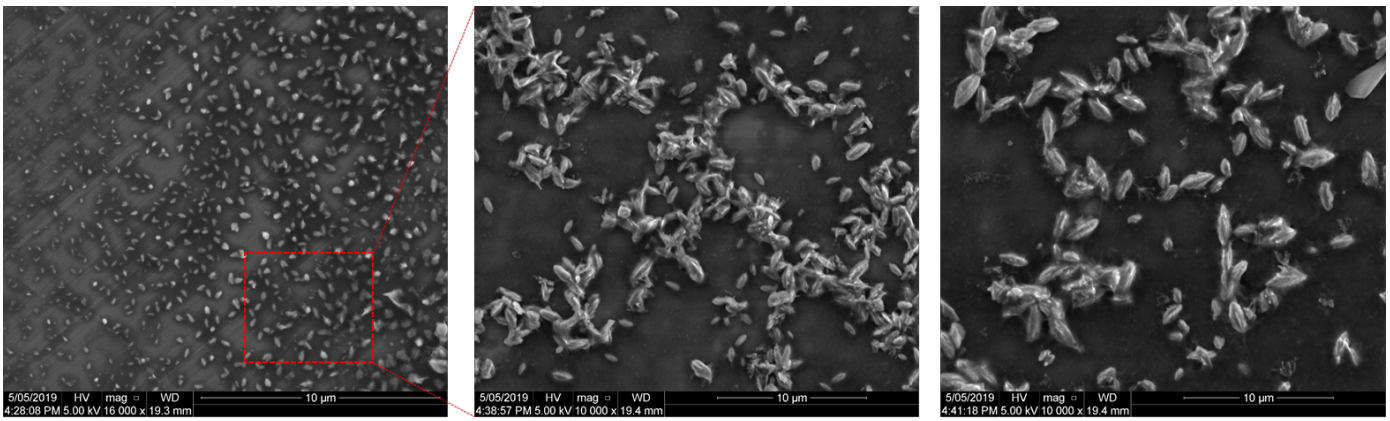

Figure S9: SEM images of graphene oxide scrolls formed in DMF in a VFD (20 mm OD, 17.5 mm ID) glass tube) at the optimised conditions; concentration of graphene oxide 0.2 mg/mL, rotational speed 4k rpm and flow rate 0.45 mL/min, θ = 45º, at room temperature.

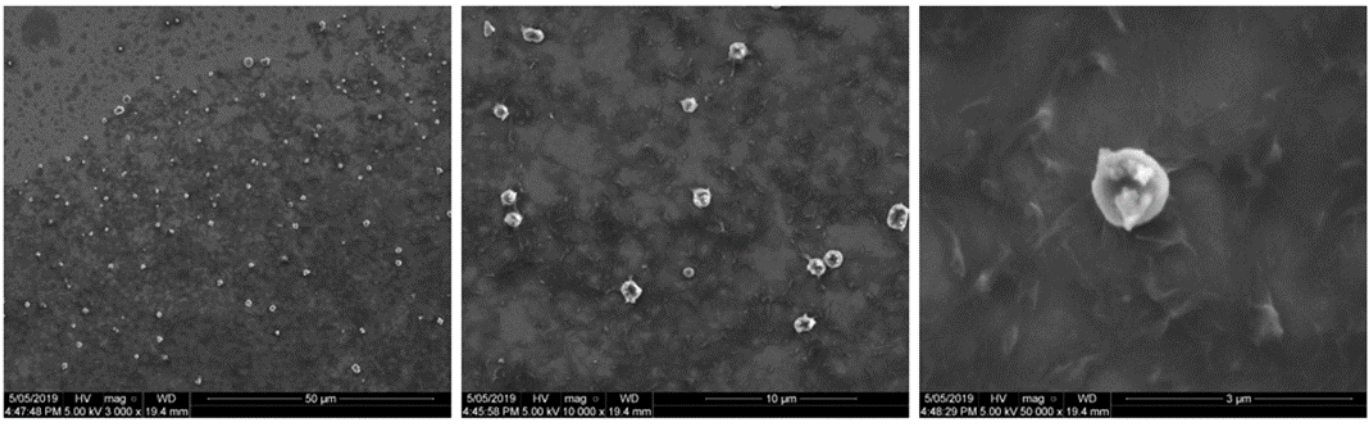

Figure S10: SEM images of crumbled graphene oxide sheets, formed in DMF in a VFD (20 mm OD, 17.5 mm ID) glass tube; concentration of graphene oxide 0.2 mg/mL, rotational speed 5k rpm (only change relative to Fig. S5a) and flow rate 0.45 mL/min, θ = 45º, at room temperature.

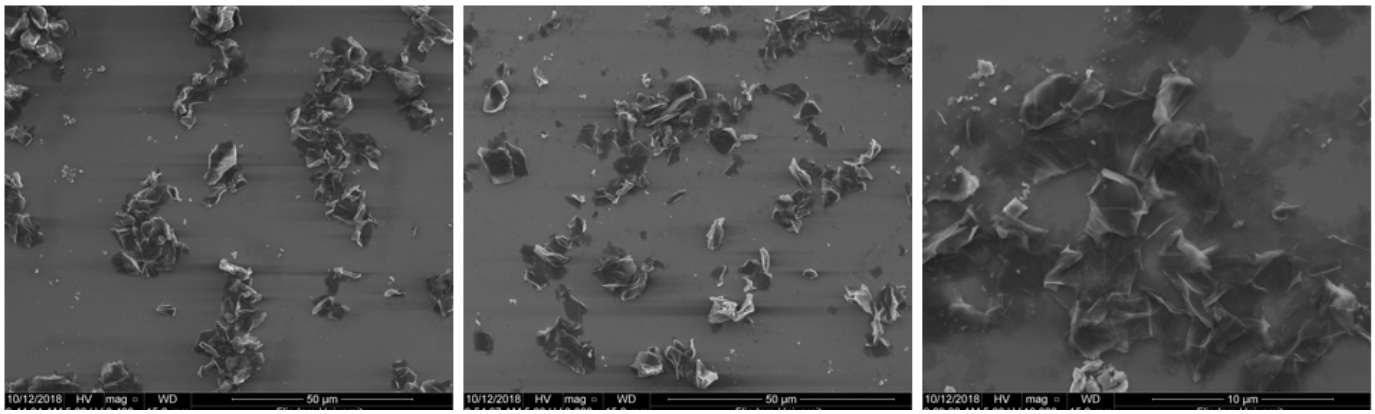

Figure S11: SEM images of crumbled graphene oxide sheets, formed in DMF in a VFD (20 mm OD, 17.5 mm ID) glass tube; concentration of graphene oxide 0.2 mg/mL, rotational speed 6k rpm (only change relative to Fig. S5a and Fig. S5b) and flow rate 0.45 mL/min, $\theta = 45^{o}$, at room temperature.

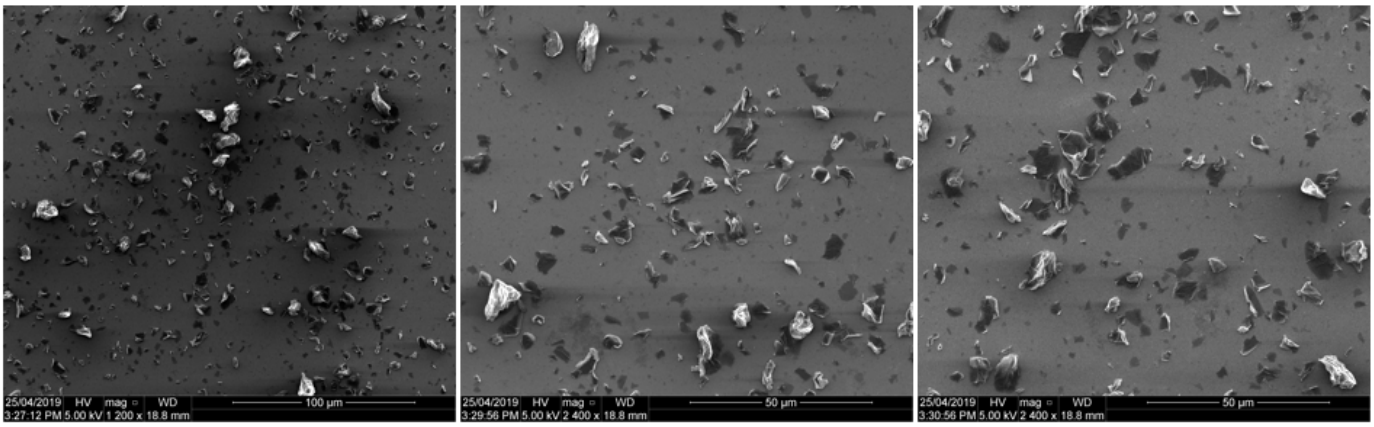

Figure S12: SEM images of crumbled graphene oxide sheets, formed in DMF in a VFD (20 mm OD, 17.5 ID glass tube); concentration of graphene oxide 0.2 mg/mL, rotational speed 7k rpm (only change relative to Fig. S5a-c) and flow rate 0.45 mL/min, $\theta = 45^{o}$, at room temperature.

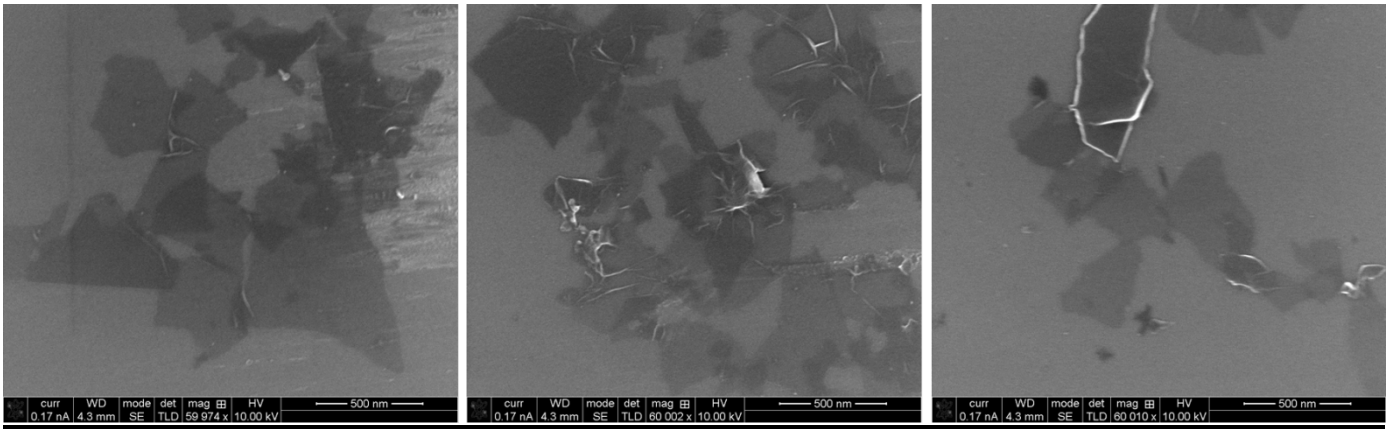

Figure S13: SEM images of crumbled graphene oxide sheets, formed in DMF in a VFD (20 mm OD, 17.5 mm ID) glass tube; concentration of graphene oxide 0.2 mg/mL, rotational speed 8k rpm (only change relative to Fig. S5a-d) and flow rate 0.45 mL/min, $\theta = 45^{o}$, at room temperature.

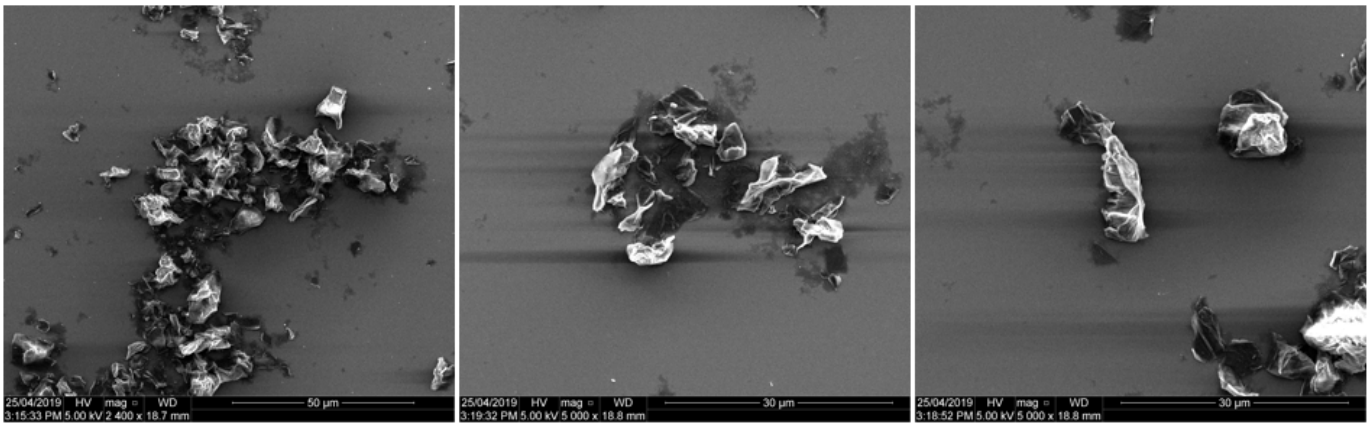

Figure S14: SEM images of crumbled graphene oxide sheets, formed in DMF in a VFD (20 mm OD, 17.5 mm ID) glass tube; concentration of graphene oxide 0.2 mg/mL, rotational speed 9k rpm (only change relative to Fig. S5a-e) and flow rate 0.45 mL/min, $\theta = 45^{o}$, at room temperature.

7. Controlling the assembly of fullerene C_{60}

Shear stress induced crystallisation of fullerene C_{60}

Fullerene C_{60} (purities of 99.5 % and 99+ %) were purchased from Sigma Aldrich and Bucky US, respectively. Toluene ≥99.9% was purchased from Sigma Aldrich. Solutions of C_{60} were prepared in toluene at different concentrations, namely 0.05, 0.1 0.2, 0.5 and 1 mg/mL. This involved adding solid material to the solvent, with the mixture left for 24 hours at room temperature. The samples were then filtered to remove undissolved particles and the supernatant was used immediately for processing in the VFD.

VFD confined mode and continuous flow processing were explored in establishing the shear stress induced crystallisation of fullerene C_{60}. For the confined mode, 1 mL of C_{60} in toluene (0.05 mg/mL, 1.0 mg/mL) was added to a VFD (20 mm OD), $\theta = 45^{o}$, and spun at different speeds for 30 min, and thereafter the liquid was collected and processed. This involved centrifugation at 1811 g, with the solid collected on a filter paper. The solid material redissolves in toluene over several hours, highlighting that there is sufficient time to collect the material with minimal re-dissolution post VFD processing. The optimal conditions were found at 5k rpm, 0.05 mg/mL, and 7.5k rpm, 1.0 mg/mL for spicules and rod like structures, respectively, Fig. S15. The concentration of C_{60} in toluene at 0.05 mg/mL, flow rate of 0.5 mL/min of the toluene solution were then used in continuous flow mode of operation of the VFD, at $\theta = 45^{o}$. At ω = 5k rpm, spicules also formed, Fig. S16 , albeit in low yield, but the yield increases on lowering the rotational speed to 4k rpm, with a further increase on increasing the concentration of C_{60} in toluene to 0.1 mg/mL, affording more spicular particles, Fig. S716 and Fig718-20. Optimal rotational speed for the formation of the rod like structures under continuous flow was also less than for confined mode, at 7k rpm, for a flow rate of 1.0 mL/min, Fig. S17. Results for changing the concentration of the fullerene in toluene, different flow rates, different tilt angles, and different rotational speeds and flow rates, are detailed in Fig. S717, Fig. S19 and Fig. S20, respectively.

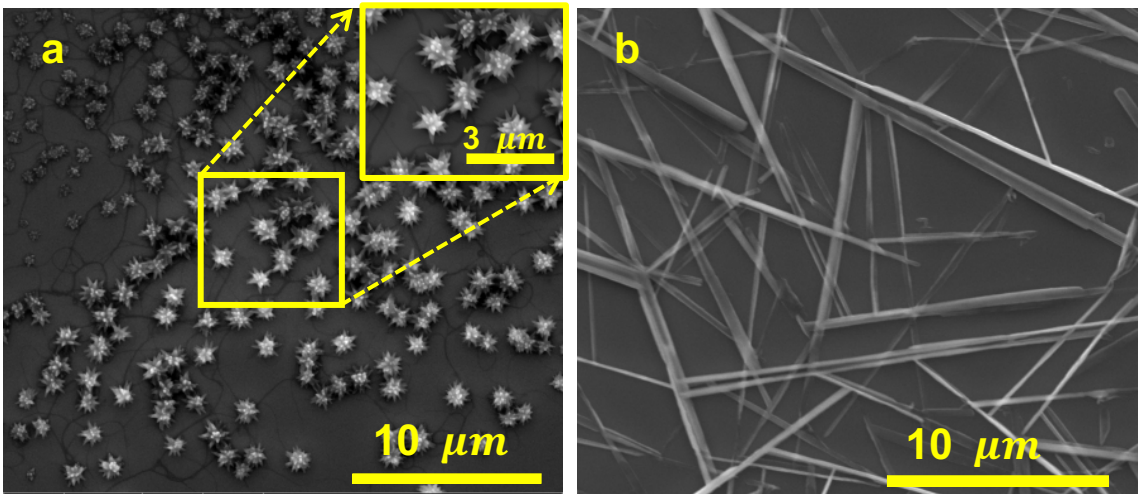

Figure S15: SEM images of C_{60} particles formed in toluene using a 20 mm OD (177.5 mm ID) VFD operating in the confined mode at (a) 4k rpm, (0.05 mg/mL) and (b) 7.5k rpm (1.0 mg/mL), θ = 45°.

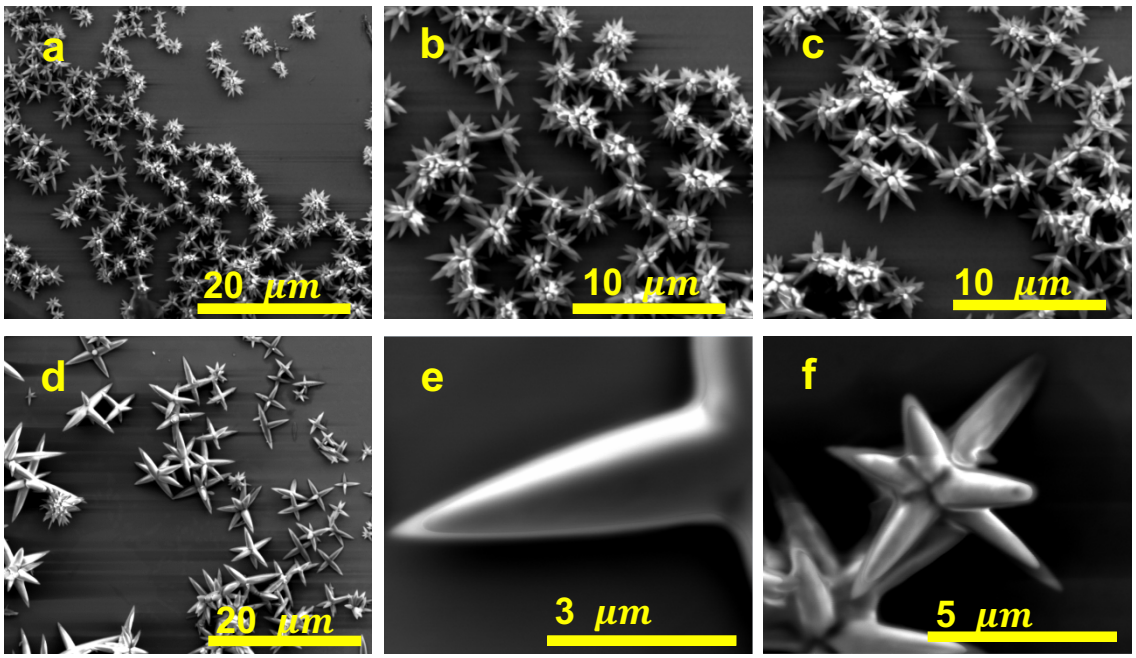

Figure S16: (a-f) SEM images of specular particles of C_{60} formed in the VFD (20 mm OD, 17.5 mm ID tube), concentration of fullerene 0.1 mg/mL, at the optimal conditions under continuous flow, 4k rpm, flow rate 0.5 mL/min, θ = 45°.

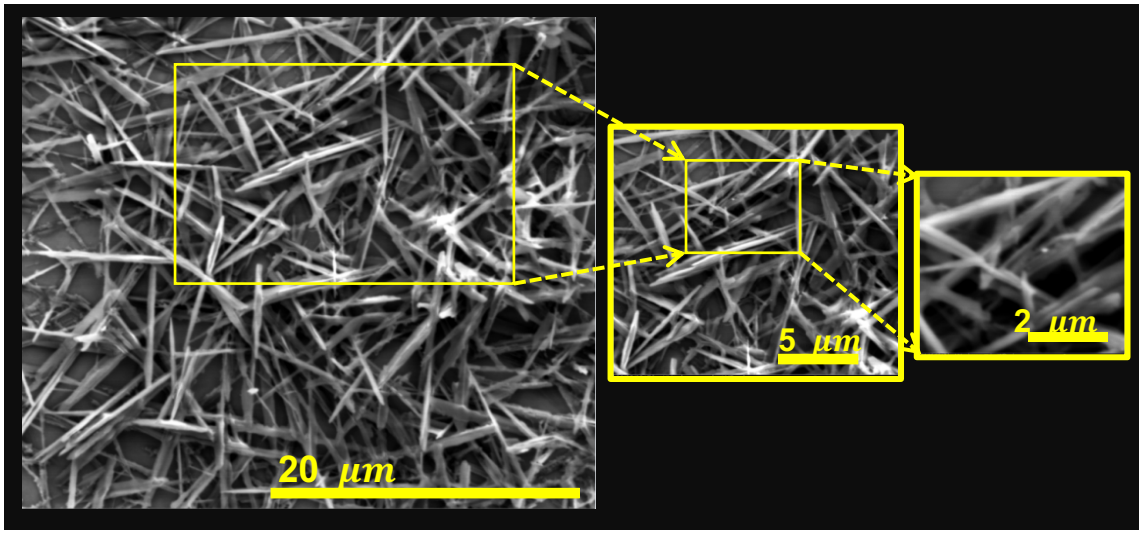

Figure S17: SEM images of shear stress induced C_{60} rod like structures, obtained from a toluene solution of C_{60} solution with the VFD tube (20 mm OD, 17.5 mm ID) rotating at 7k rpm, concentration 0.1 mg/mL, flow rate 1 mL/min and $\theta = 45^{o}$.

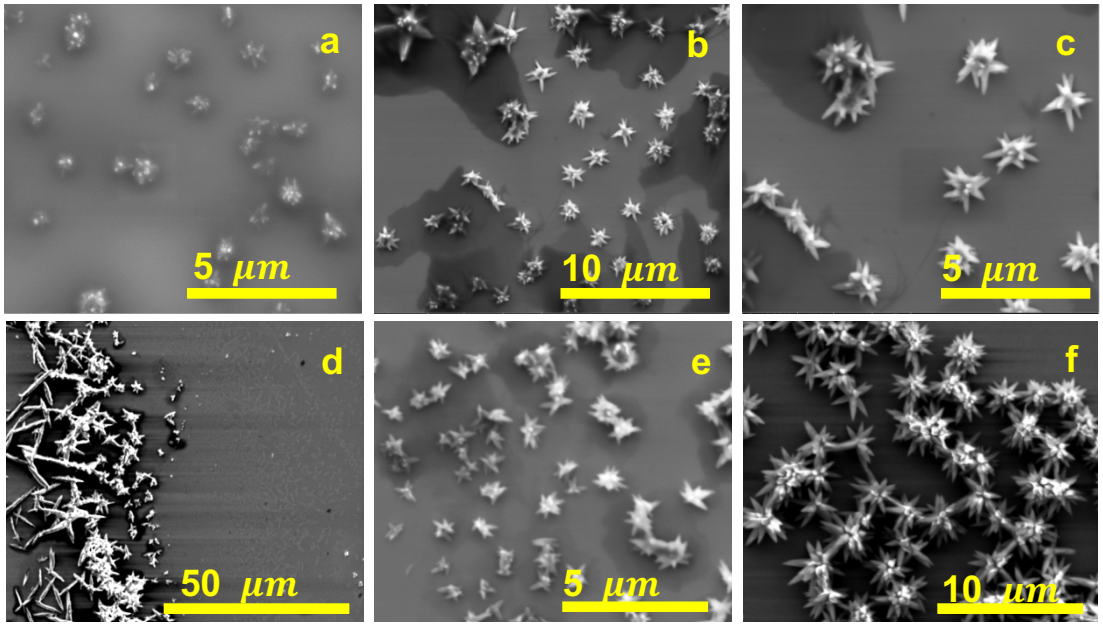

Figure S18: SEM images of spicules of fullerene C_{60} formed in the VFD (20 mm OD, 17.5 mm ID tube) in a solution of the fullerene in toluene, (a) ω = 5k rpm, $\theta = 45^{o}$, 0.05 mg/mL, 0.5 mL/min, (b,c) ω = 4k rpm, 0.05 mg/mL, 0.5 mL/min , (d) ω = 3k rpm, 0.1 mg/mL, 1.0 mL/min, (e) ω = 4k rpm, 0.05 mg/mL, 0.1 mL/min, and (f) ω = 4k rpm, 0.1 mg/mL, 0.1 mL/min.

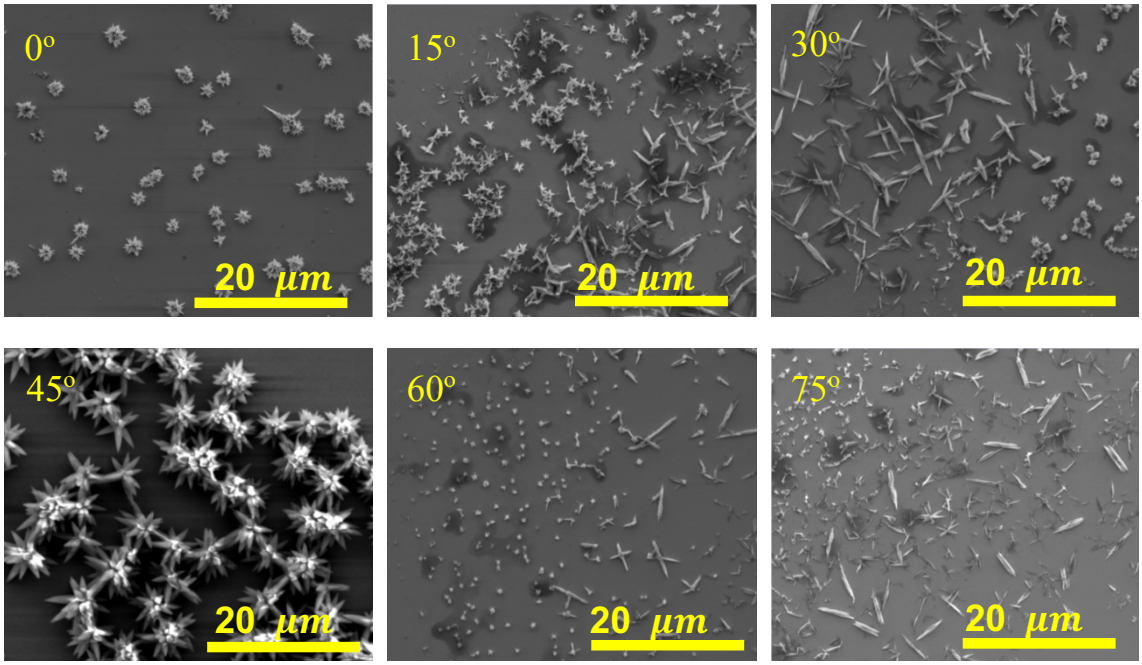

Figure S19: SEM images of material formed under shear stress in the VFD (20 mm OD, 17.5 mm ID) in C_{60} solutions of toluene, 0.1 mg/mL, ω = 4k rpm, at different tilt angles, θ, as specified.

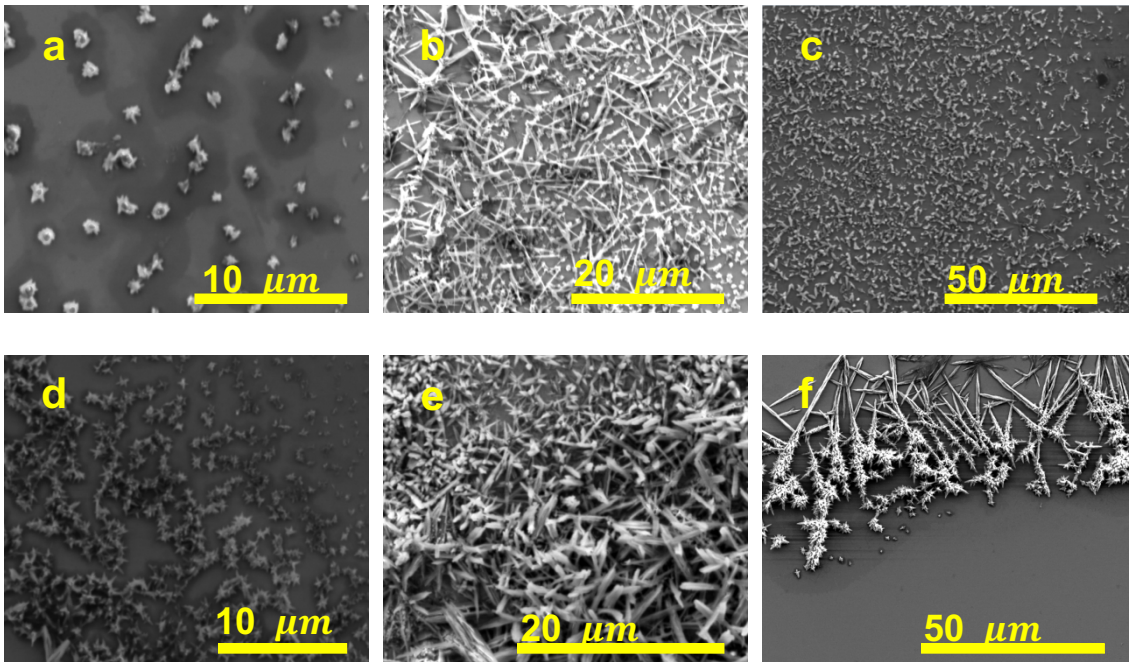

Figure S20: (a-f) SEM images of shear stress induced nanoparticles of C_{60} formed from a solution of the fullerene in toluene, 0.1 mg/mL, at θ = 45°, at different speeds and flow rates (a) 3k rpm, 0.5 mL/min, (b) 6k rpm, 0.5 mL/min, (c) 9k rpm, 1 mL/min, (d) 3k, 0.1 mL/min, (e) 6k rpm, 0.1 mL/min, (f) 3k rpm, 1.0 mL/min.

Visible spectroscopy studies on toluene solutions of fullerene C_{60} immediately post-VFD processing under continuous flow.

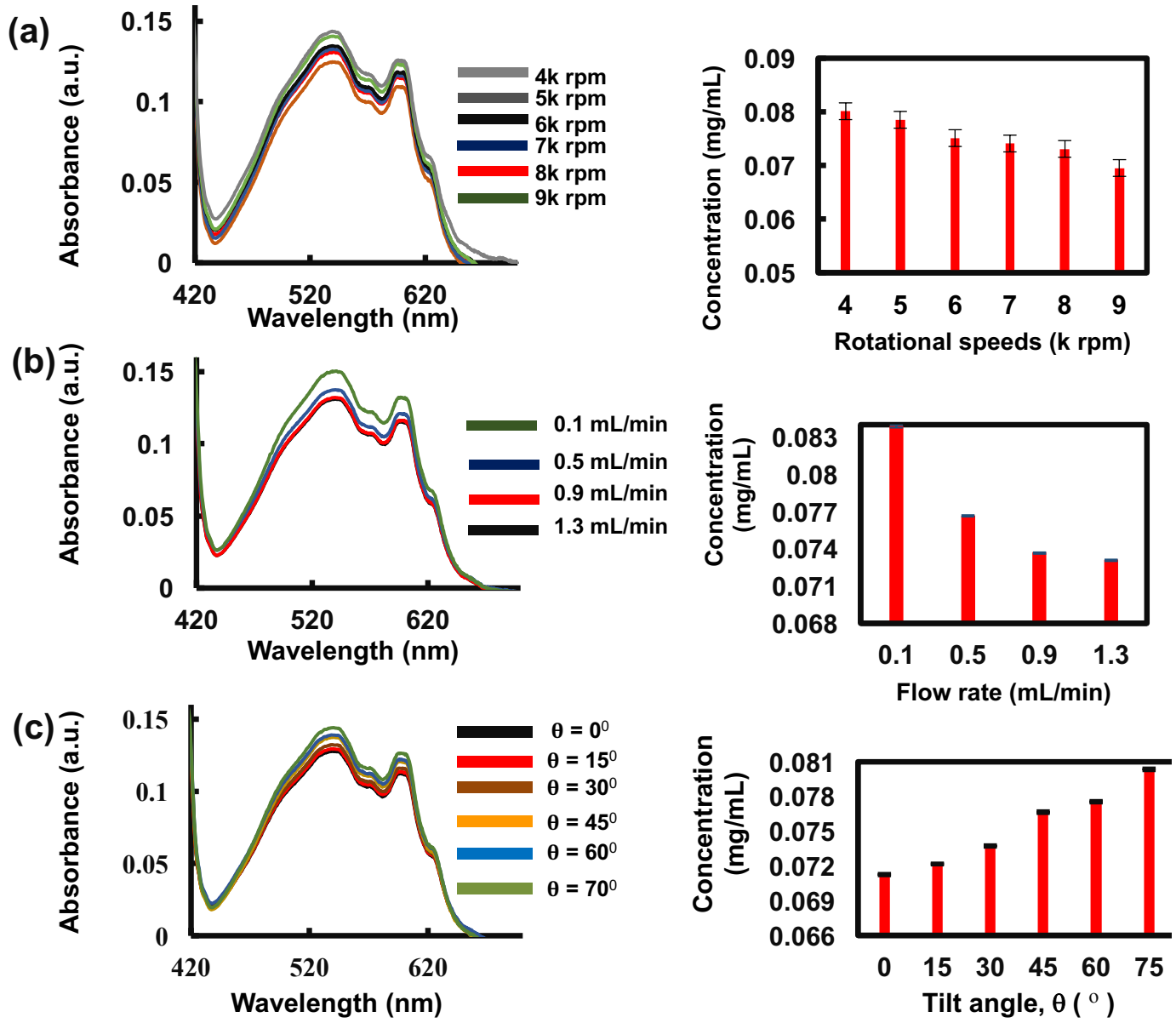

Figure S21: Visible spectra and residual concentrations of toluene solutions of C_{60} immediately post-processing in the VFD (20 mm OD, 17.5 mm ID), as a function of (a) different rotational speeds, concentration 0.1 mg/mL, θ = 45°, flow rate 0.1 mL/min, (b) different flow rates, concentration 0.1 mg/mL, θ = 45°, ω = 4k rpm, and (c) different tilt angles, concentration 0.1 mg/mL, flow rate 0.1 mL/min, ω = 4k rpm (Left). (Right) Concentration of residual C_{60} as a function of rotational speed, flow rate and tilt angle, as determined using $A = \varepsilon l c$ (ε molar absorptivity, l, path length and c concentration), based on a molar absorptivity, ε, of 933 $M^{-1}.cm^{-1}$ for C_{60} in toluene at 540 nm[1].

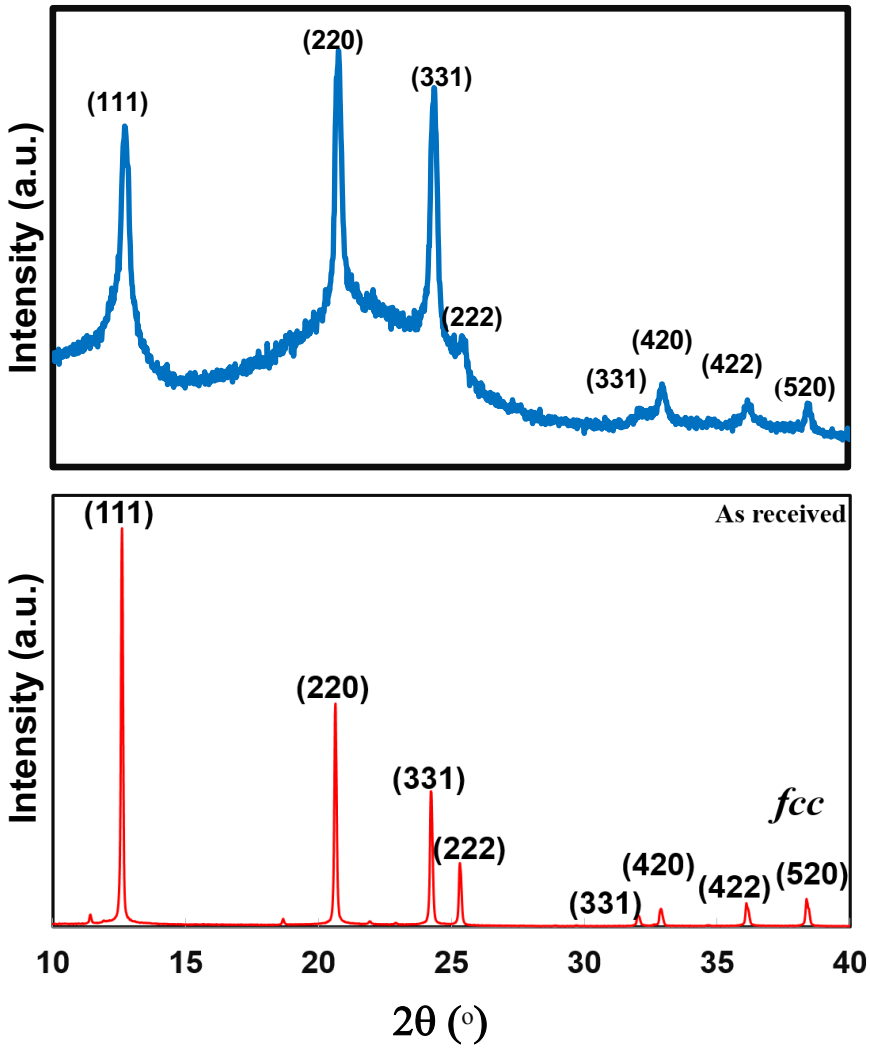

Figure S22: X-ray diffraction pattern for the spicules formed at the optimal conditions, 0.1 mg/mL of C_{60} in toluene, ω = 4k rpm, flow rate 0.5 mL/min, θ = 45° (top) versus as received C_{60} (bottom).

Fullerene C_{60} cones

The synthesis of fullerene C_{60} cones follows the published procedure[2] using a 20 mm OD tube, herein adapted for a 10 mm OD (8.5 mm ID) glass tube operating under continuous flow conditions, using 2 jets feeds delivering equal amounts of liquid to the base of the tube, with one jet delivering an *o*-xylene solution of C_{60} and the other DMF as the anti-solvent.

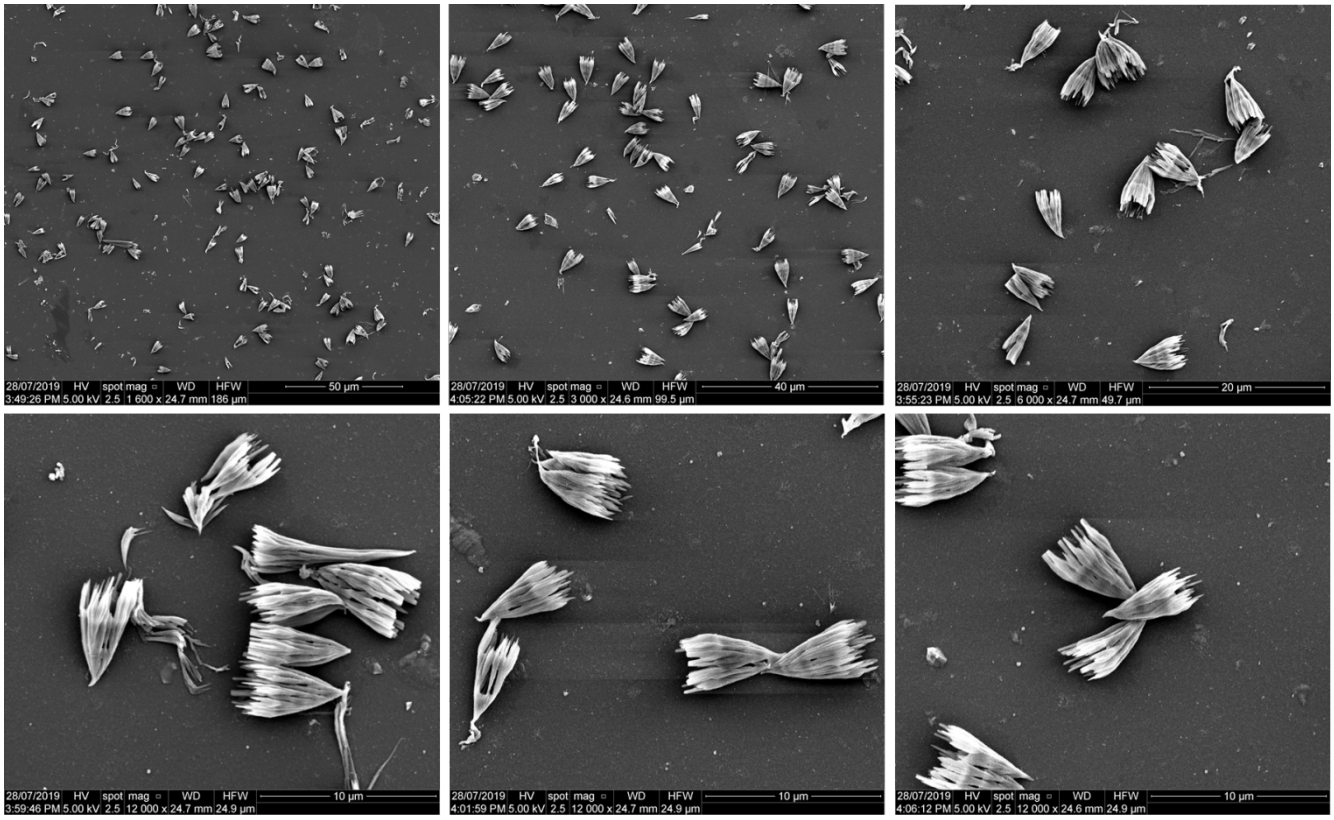

Figure S23: SEM images of C_{60} cones formed on micromixing a 1:1 solution of *o*-xylene solution of C_{60} (0.1 mg/mL, flow rate 0.1 mL/min) and DMF (0.1 mL/min) in a 10 mm OD VFD tube, ω = 4k rpm, θ 45º, the product being collected by centrifugation at 1180 × *g* and washed with hexane, then air dried.

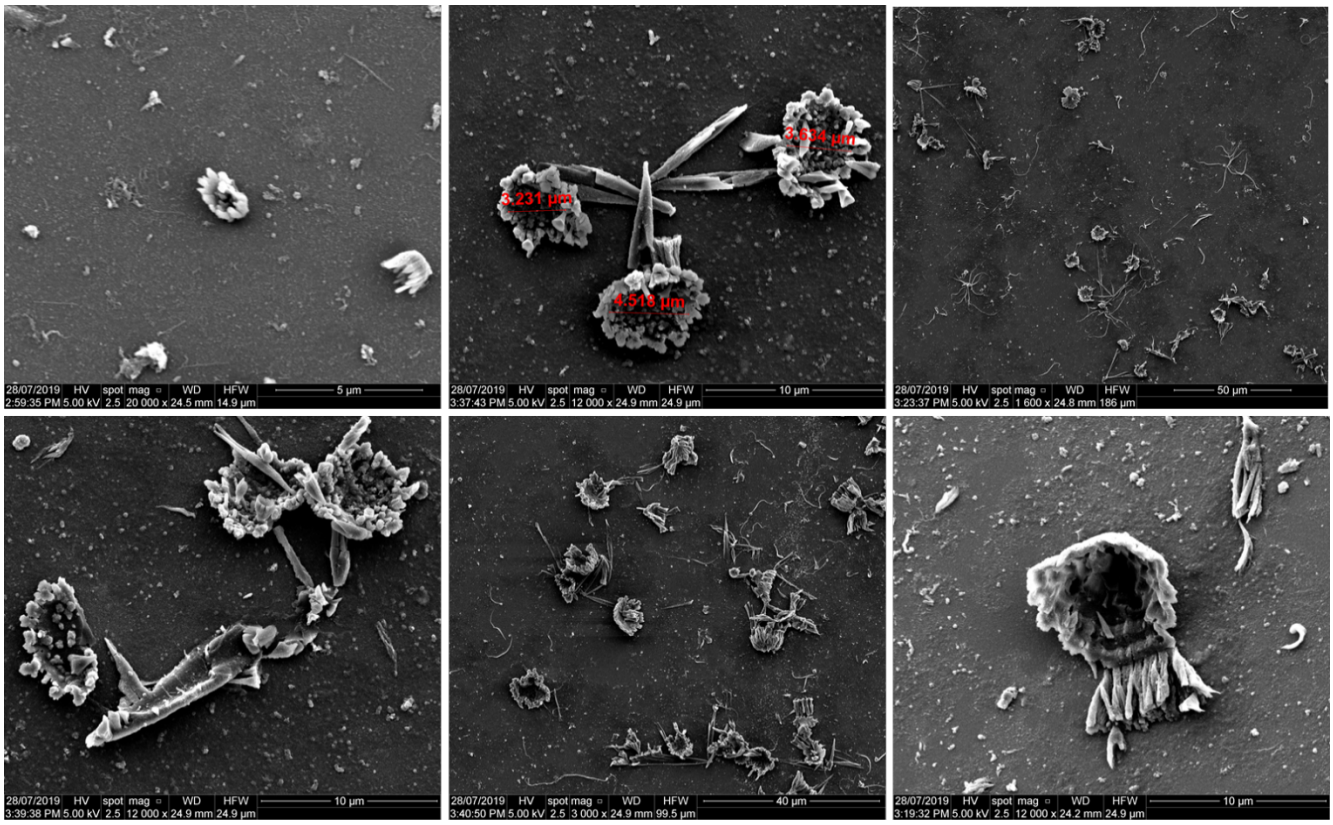

Figure S24: SEM images of C_{60} cones and other material located on the inner surface of the 10 mm OD glass tube following the processing in Fig. S7a (micromixing a 1:1 solution of *o*-xylene solution of C_{60} (0.1 mg/mL, flow rate 0.1 mL/min) and DMF (0.1 mL/min) in a 10 mm OD VFD tube, ω = 4k rpm, θ 45°).

8. Moulding of polysulfone (PSF) in the VFD

Different concentrations of a PSF solutions were explored to generate a uniform thin-film adhering to the inner surface of the tube. Ultimately this led to using 1 mL of 50 mg/ml of PSF dissolved in dichloromethane (DCM) to generate such a film, Fig. S24. This involved adding a solution of the polymer to a VFD tube (20 mm OD, 17.5 mm ID) tilted at 5° which was then spun at 6k rpm for ~15 min. Evaporation was facilitated by high mass and heat transfer in the tube which was left open to the atmosphere. The film was washed several times with hexane and then dried under a flow of dry nitrogen. Sections of the film was then peeled from the surface of the tube at three different locations, Figure S25. Fig. S26 shows that the thin film created in the VFD is relatively uniform with occasional deformations on the upper surface (air contact) whereas the lower surface (glass contact) is smooth - devoid of any structure variation.

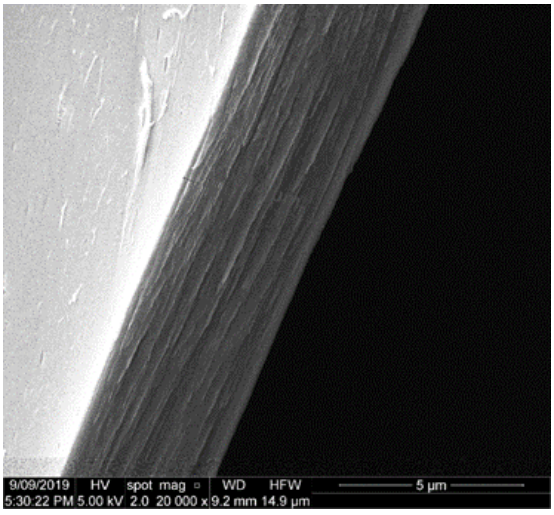

Figure S25: SEM image of the thin-film of PSF created in the VFD tube (20 mm OD, 17.5 mm ID) at 6k rpm rotational speed, $\theta = 5°$ and room temperature during 15 min, after adding 1 mL of 50 mg/ml of PSF dissolved in DCM.

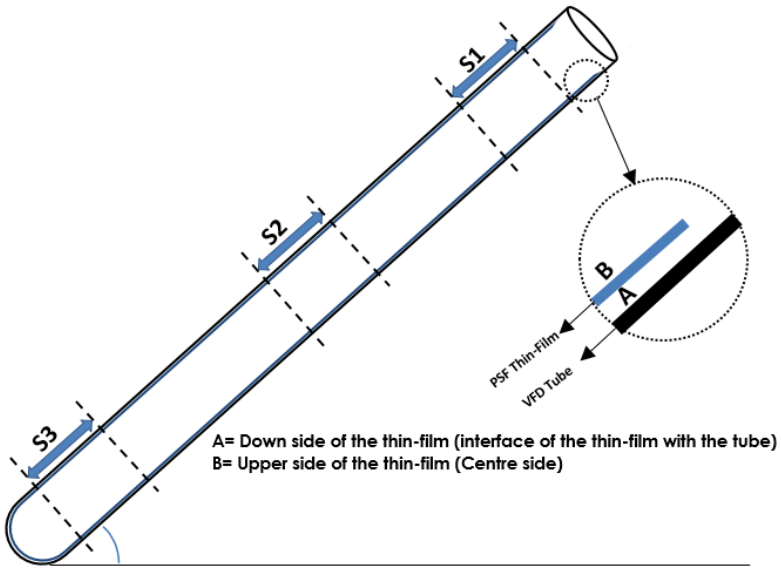

Figure S26: Locations of samples S1, S2 and S3 taken from the PSF thin-film formed in the VFD; sample S1A and S1B refer to the interface of film with the tube and air from the bottom of the tube respectively, and similarly S2A and S2B, and S3A and S3B, from the middle and top of the tube

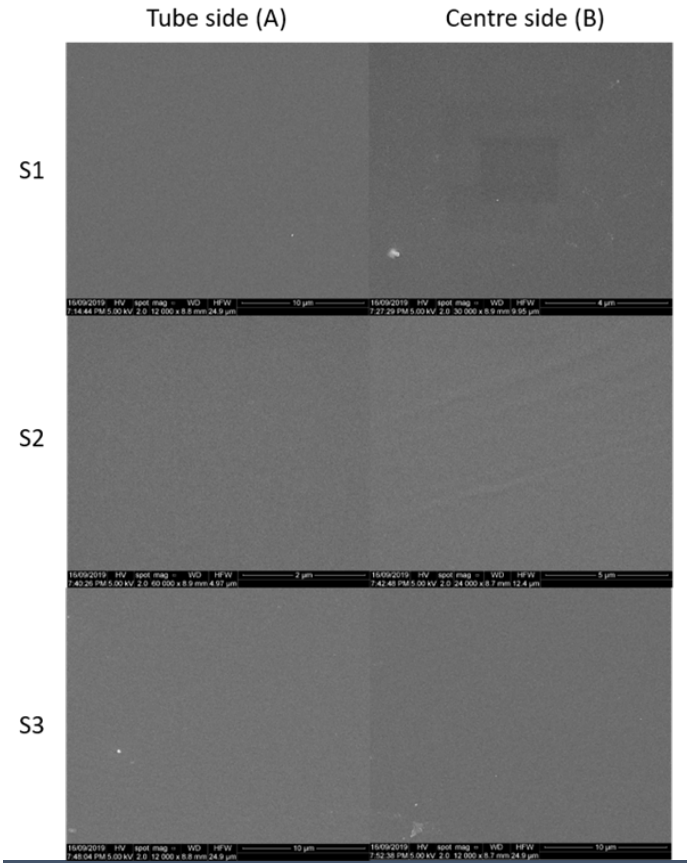

Figure S27: SEM images of S1, S2, and S3 from both sides (left: bottom of the thin film, right; upper side of the thin-film) of a thin-film created in the VFD (20 mm OD tube) at 6k rpm, θ = 5°, at room temperature during 15 min of processing.

Toluene and water (0.5 mL) were independently added to a VFD tube coated with a thin film of PSF, in which the polymer is only sparingly soluble, and the tube was rotated at 7k rpm at θ = 45°, at room temperature, for one hour. After processing, the liquid was drained, and the film washed with hexane several times and purged with nitrogen gas for drying purposes, for 2h. A section of the film was removed from the middle of each tube and studied using SEM, Fig. S27 and S28, for toluene and water respectively, with the red arrow essentially parallel to the rotation axis of the tube when θ = 45°, and in the direction of the upper lip. This revealed arrays of indentations and some holes on the side A of the polymer film processed in toluene, with a limited number of such structures for water. SEM imaging the other side of the PSF film (side B) post-VFD processing using the same conditions revealed smooth surface, for both toluene or water (Fig. S29). Given the structures revealed on surface SA for toluene, all subsequent processing was done in toluene followed by washing with hexane, and as a control, processing in toluene and not washing with hexane afforded the same morphology, Fig. S32. The change in morphology of the surface of the PSF film that was in contact with the glass during VFD in toluene provides information on the fluid behavior, as shown diagrammatically in Fig. 1.

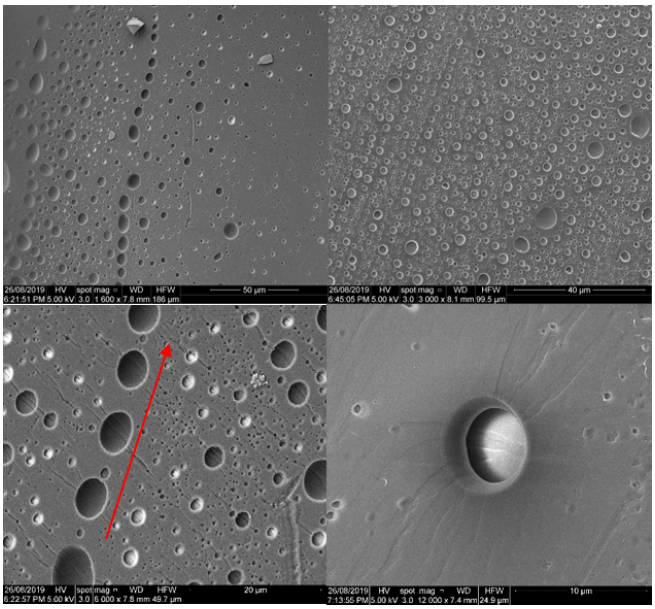

Figure S28: SEM images of the central inner surface of the film (S2A) after VFD processing (20 mm OD, 17.5 mm ID tube) in toluene, at room temperature ω = 7k rpm, θ = 45° for ~1h, after washing with hexane.

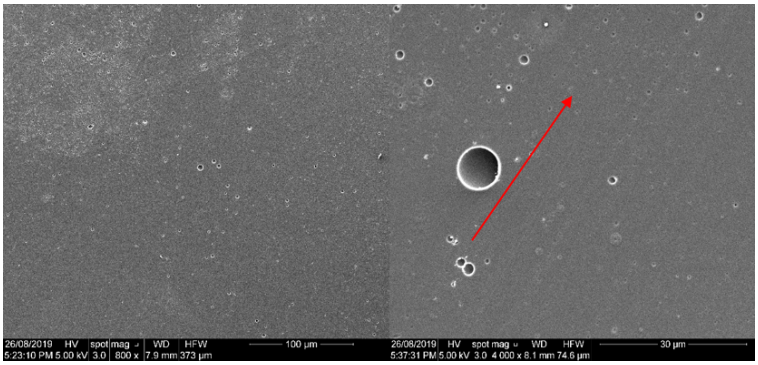

Figure S29: SEM images of the central inner surface of the film (S2A) after VFD processing (20 mm OD tube) in water, at room temperature, ω = 7k rpm, θ = 45°, for ~1h, after washing with hexane.

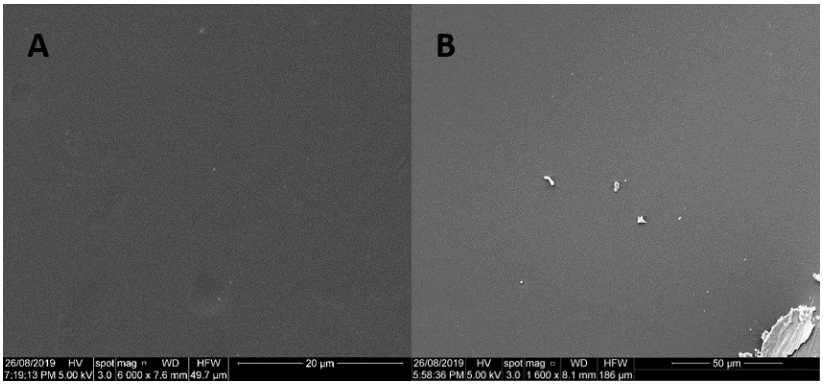

Figure S30: SEM images of the central upper surface (S2B) after VFD processing (20 mm OD tube) in water, at room temperature ω = 7k rpm, θ = 45° for ~1h, in (A) toluene and (B) water, after washing with hexane and drying with nitrogen gas for 2h

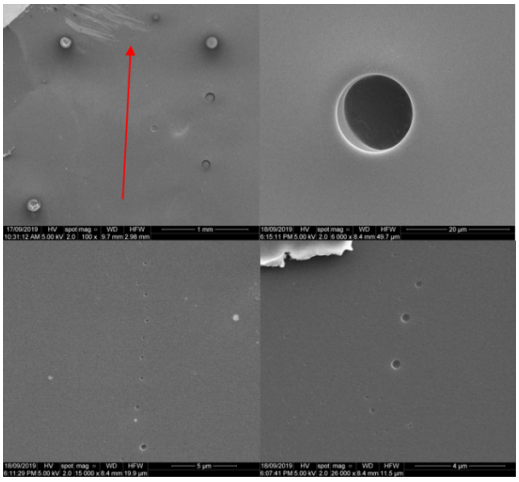

Figure S31: SEM images of the central inner surface of the film (S2A) after VFD processing (20 mm OD tube) in toluene, at room temperature ω = 7k rpm, θ = 45° for ~1h, and drying with nitrogen gas for 2h, without washing with hexane prior to SEM imaging.

Molecular drilling control experiment

Table S1: Control experiments for determining the 'molecular drilling' on a PSF thin film in the VFD tube, in high shear fluid flow at room temperature.*

Sample	**Rotational Speed (k rpm)**	**θ (°)**	**Volume of Toluene (mL)**	**Time (min)**
Thin-film	6k	5	----	15
1	7k	45	0.85	30
2	5k	45	1.9	30
3	3.5	45	5	30
4	7	30	0.75	30
5	5	30	1.7	30
6	3.5	30	4.7	30
7	7	60	1	30
8	5	60	2.1	30
9	3.5	60	5.4	30

* Notes:

(i) The first entry is for creating the PSF thin-film in a VFD tube (20 mm OD, 17.5 mm ID) from a solution of the polymer in dichloromethane at 6k rpm, with θ = 5° to ensure the film is formed close to the full length of the tube during the evaporation of the solvent, ca 15 min.

(ii) The volume of polymer solution for each sample corresponds to that required to create a film across the entire length of the tube at θ = 5°, with the then 'molecular drilling' experiments carried out at θ = 30, 45 and 60°.

(iii) The films of PSF in the VFD were washed with hexane and purged with nitrogen gas prior to peeling off the glass tube.

(iv) Three sections of the films (S1, S2 and S3, Fig. S25) were taken from every sample, with both sides (A and B) studied using SEM, affording six images for each sample, designated S1A, S2A, S3A, S1B, S2B and S3B, as elaborated below.

Thin-film

Rotational speed : 6k rpm

Tilt angle, q θ : 5°

Solvent : CH_2Cl_2

Time : 15 min

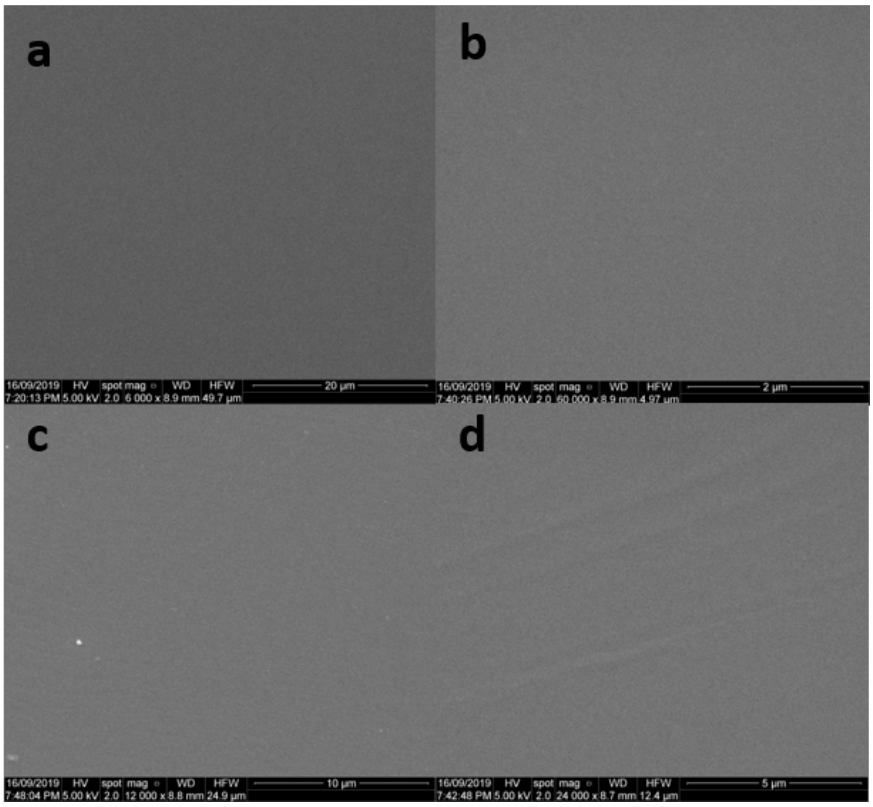

Figure S32: SEM images of PSF thin-film created in the VFD tube (20 mm OD) at 6k rpm, θ = 5° at room temperature during 15 min of evaporation of DCM: (a) S1A, (b) S2A, (c) S3A and (d) S2B, revealing smooth surfaces present, prior to processing in toluene.

Sample 1:

Rotational speed : 7k rpm

Tilt angle, θ : 45°

Solvent : Toluene

Time : 30 min

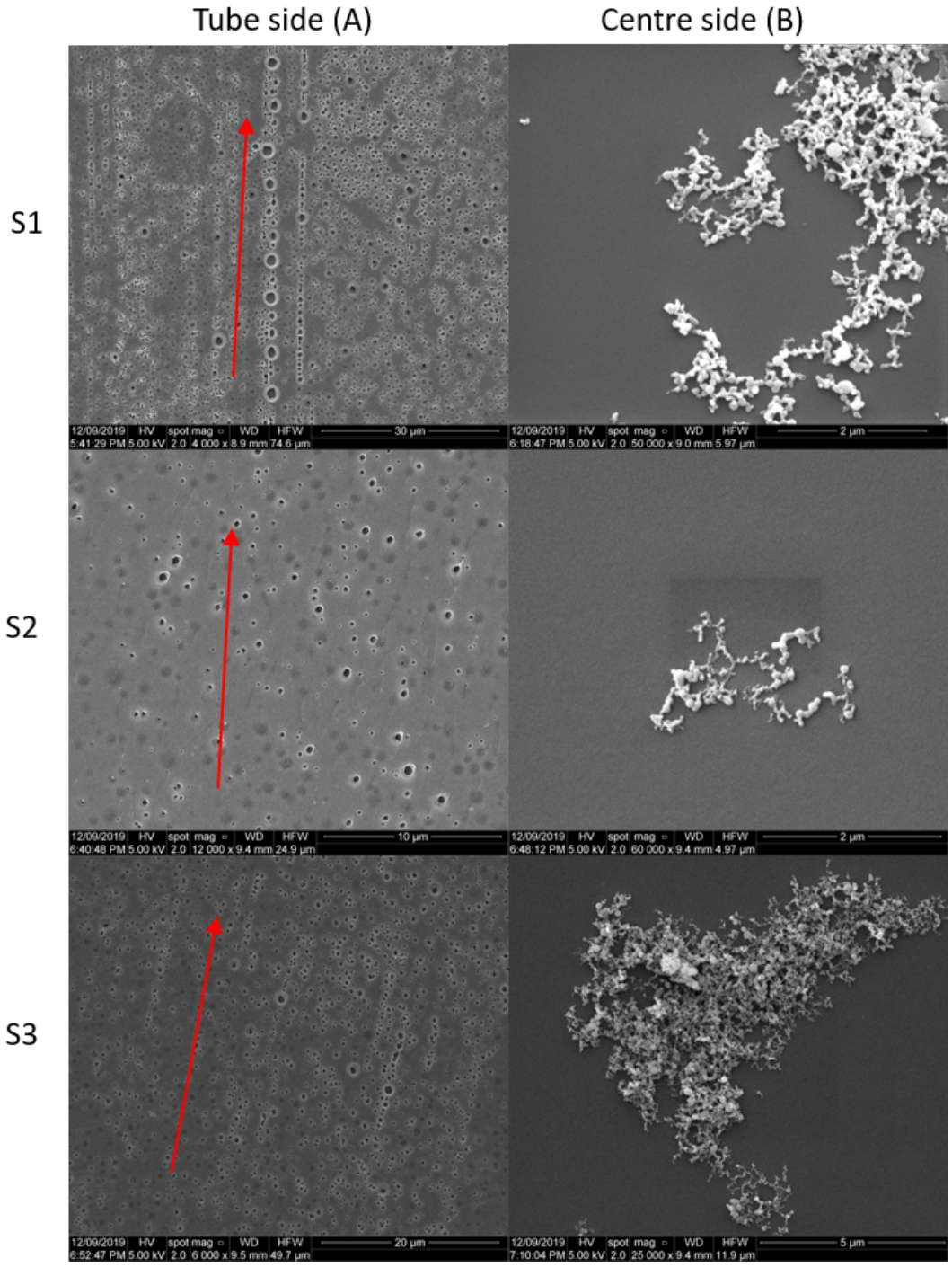

Figure S33: SEM images of S1, S2, and S3 from both sides (left: bottom of the thin film (A), right; upper side of the thin-film (B) of the thin-film processed in toluene at 7k rpm, θ = 45°, room temperature, and 30 min processing, then washed with hexane, and dried under nitrogen gas. The red arrows define the direction of rotation of the axis of the tube, directed out of the tube.

Sample 2:

Rotational speed : 5k rpm

Tilt angle, θ : 45°

Solvent : Toluene

Time : 30 min

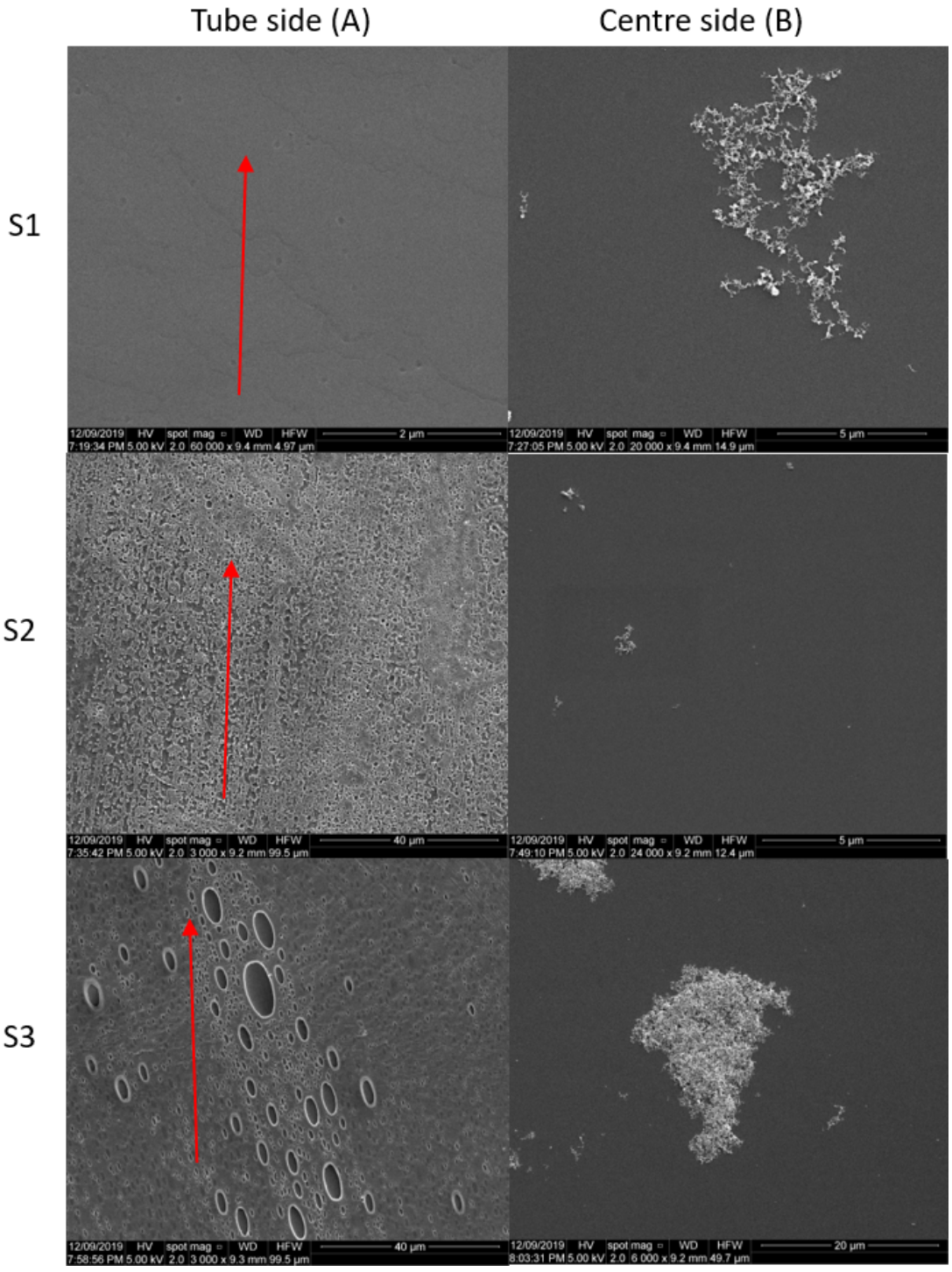

Figure S34: SEM images of S1, S2, and S3 from both sides (left: bottom of the thin film (A), right; upper side of the thin-film (B) of the thin-film processed in toluene at 5k rpm, θ = 45°, room temperature, and 30 min processing, then washed with hexane, and dried under nitrogen gas. The red arrows define the direction of rotation of the axis of the tube, directed out of the tube.

Sample 3:

Rotational speed : 3.5k rpm

Tilt angle, θ : 45°

Solvent : Toluene

Time : 30 min

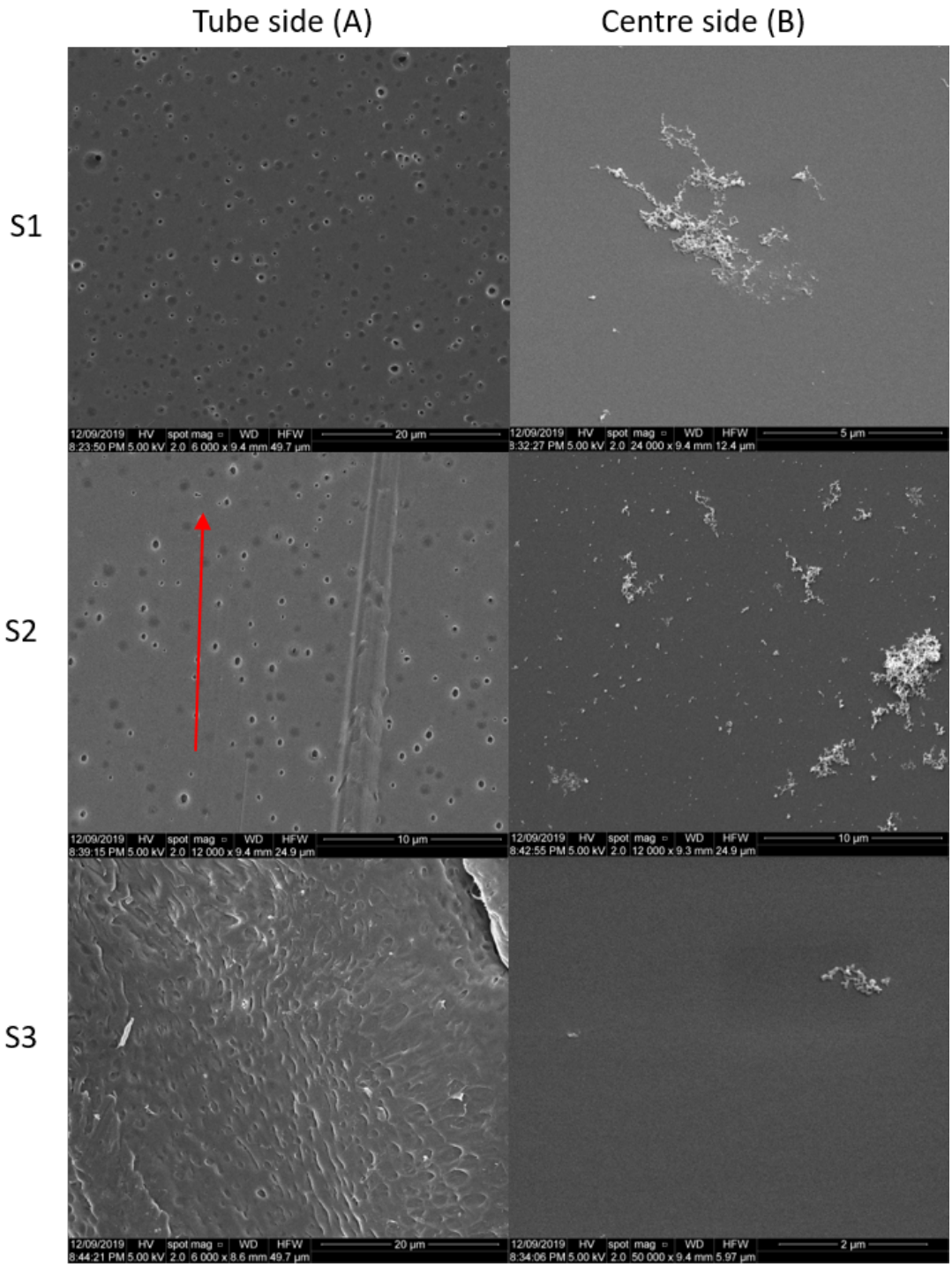

Figure S35: SEM images of S1, S2, and S3 from both sides (left: bottom of the thin film (A), right; upper side of the thin-film (B) of the thin-film processed in toluene at 3.5k rpm, θ = 45°, room temperature, and 30 min processing, then washed with hexane, and dried under nitrogen gas. The red arrow defines the direction of rotation of the axis of the tube, directed out of the tube.

Sample 4:

Rotational speed : 7k rpm

Tilt angle, θ : 30°

Solvent : Toluene

Time : 30 min

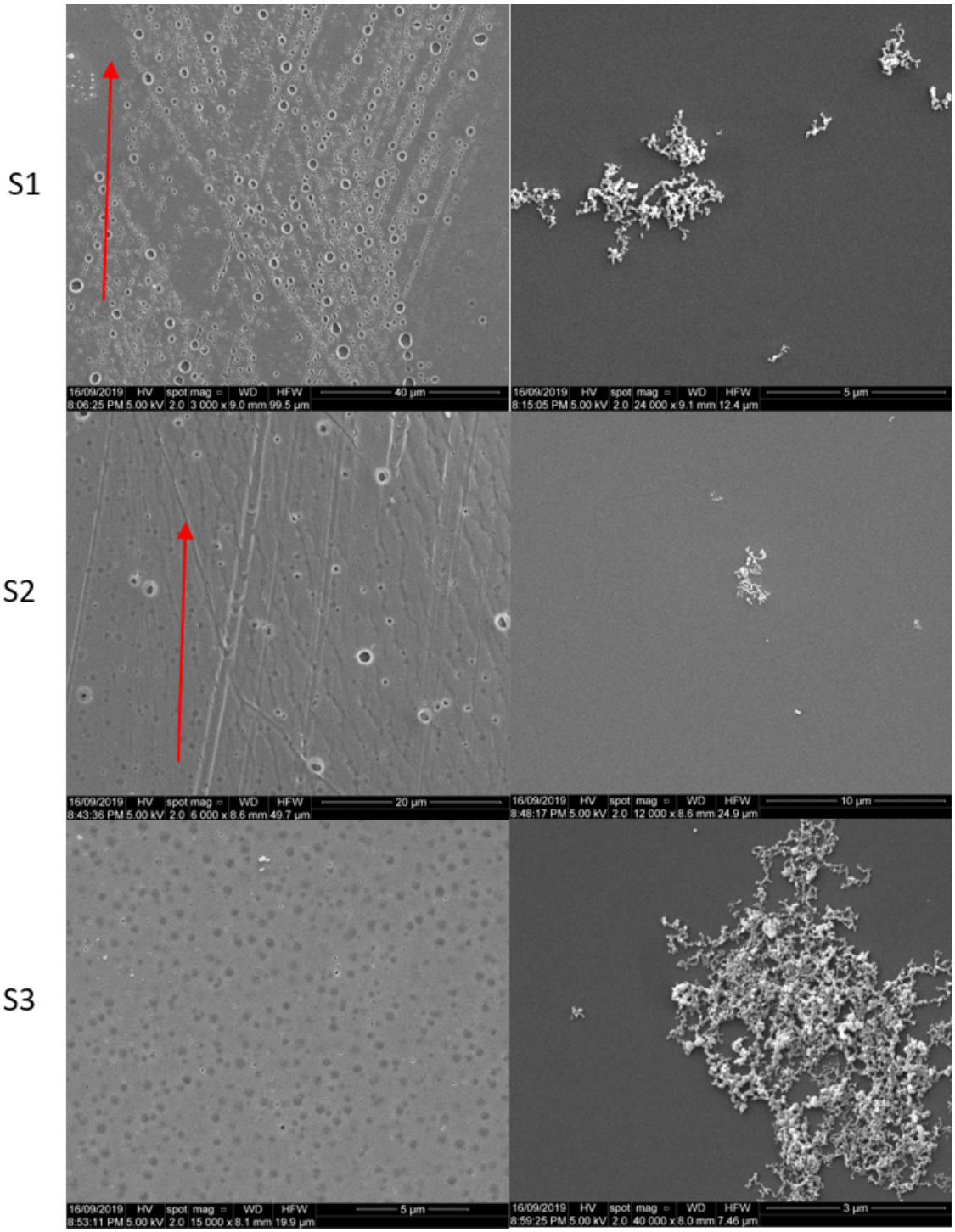

Figure S36: SEM images of S1, S2, and S3 from both sides (left: bottom of the thin film (A), right; upper side of the thin-film (B) of the thin-film processed in toluene at 7k rpm, θ = 30°, room temperature, and 30 min processing, then washed with hexane, and dried under nitrogen gas. The red arrows define the direction of rotation of the axis of the tube, directed out of the tube.

Sample 5:

Rotational speed : 5k rpm

Tilt angle, θ : 30°

Solvent : Toluene

Time : 30 min

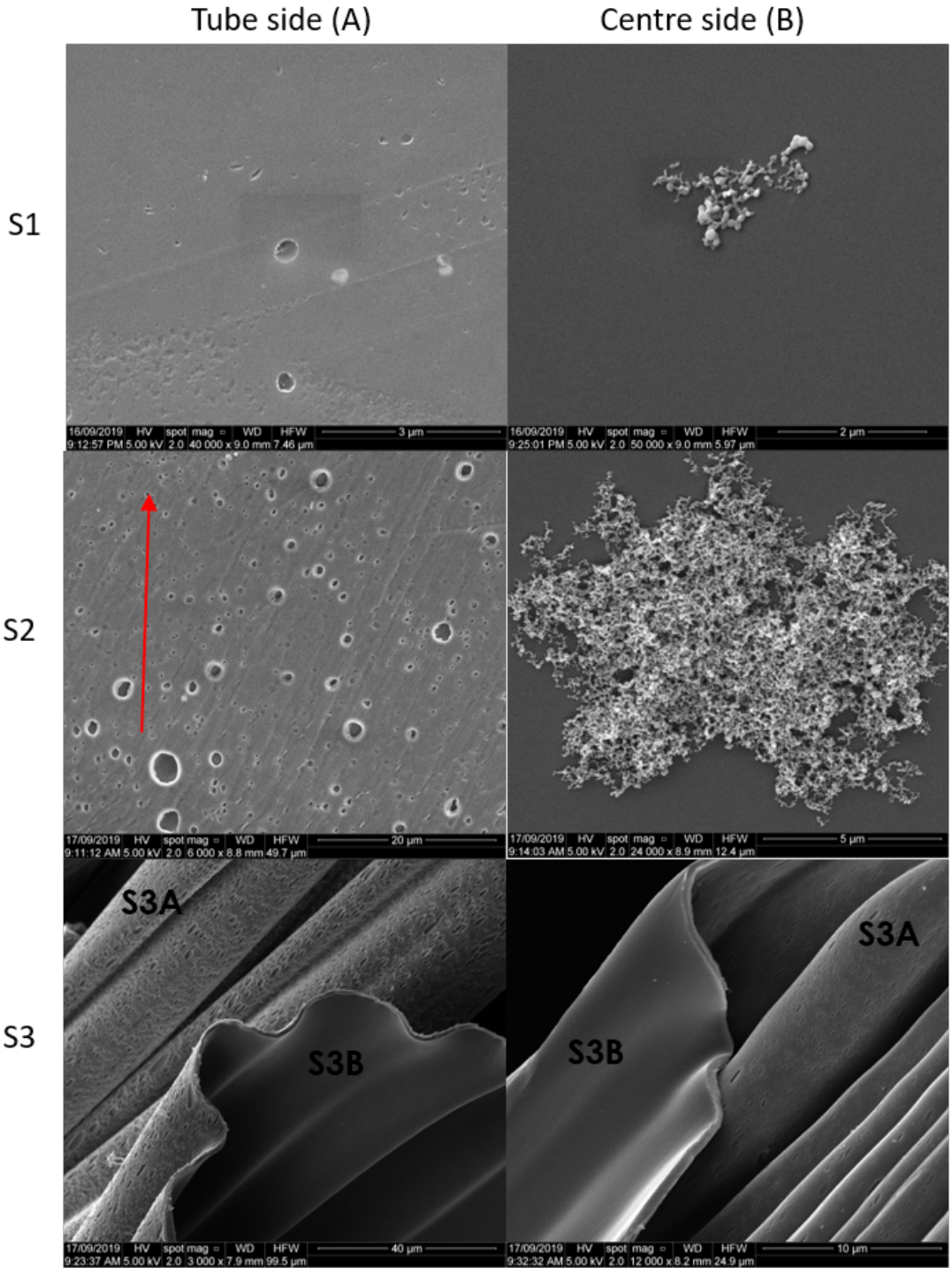

Figure S37: SEM images of S1, S2, and S3 from both sides (left: bottom of the thin film (A), right; upper side of the thin-film (B) of the thin-film processed in toluene at 5k rpm, θ = 30°, room temperature, and 30 min processing, then washed with hexane, and dried under nitrogen gas. The red arrow defines the direction of rotation of the axis of the tube, directed out of the tube.

Sample 6:

Rotational speed : 3.5k rpm

Tilt angle, θ : 30°

Solvent : Toluene

Time : 30 min

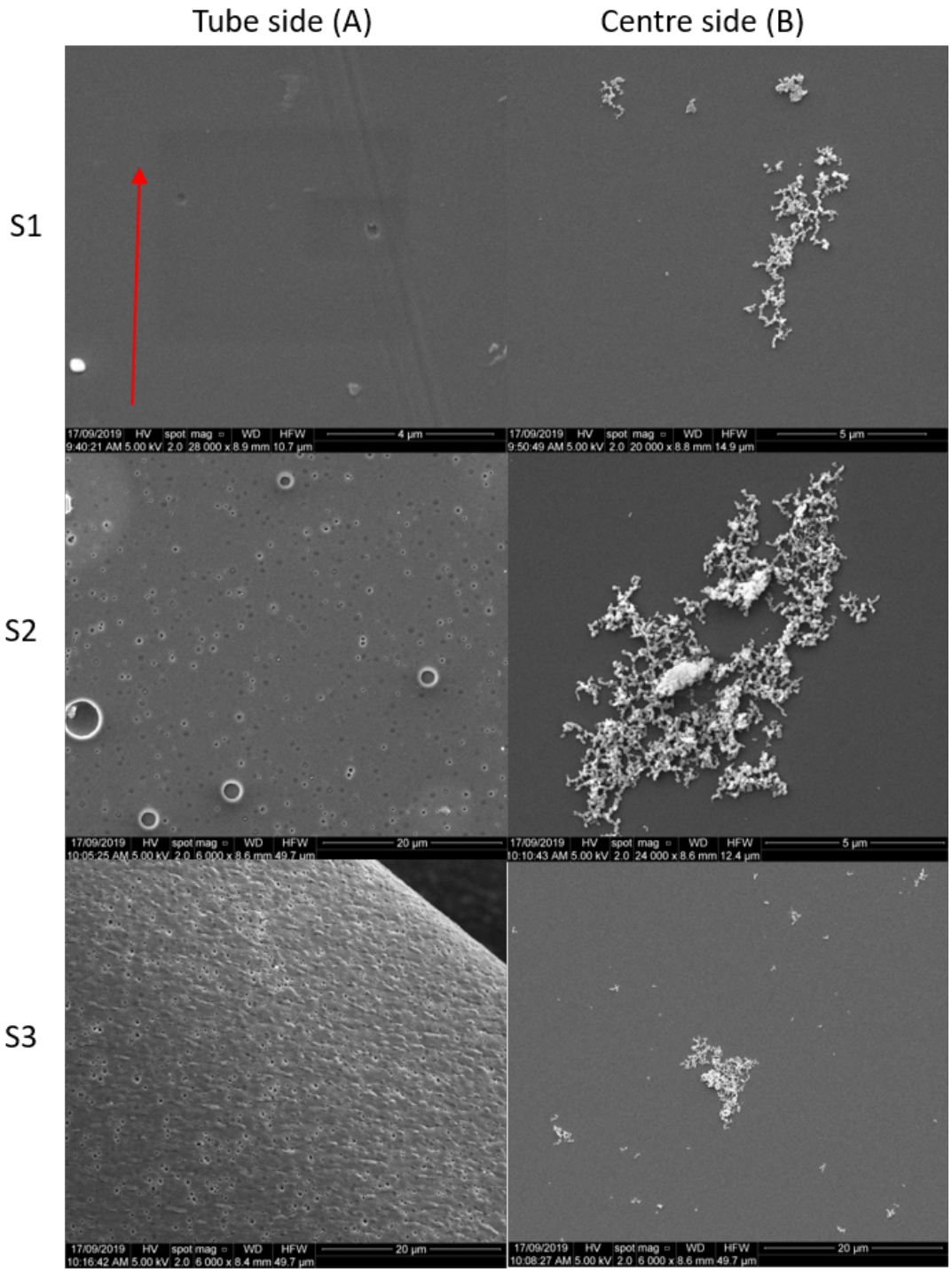

Figure S38: SEM images of S1, S2, and S3 from both sides (left: bottom of the thin film (A), right; upper side of the thin-film (B) of the thin-film processed in toluene at 3.5k rpm, θ = 30°, room temperature, and 30 min processing, then washed with hexane, and dried under nitrogen gas. The red arrow defines the direction of rotation of the axis of the tube, directed out of the tube.

Sample 7:

Rotational speed : 7k rpm

Tilt angle, θ : 60°

Solvent : Toluene

Time : 30 min

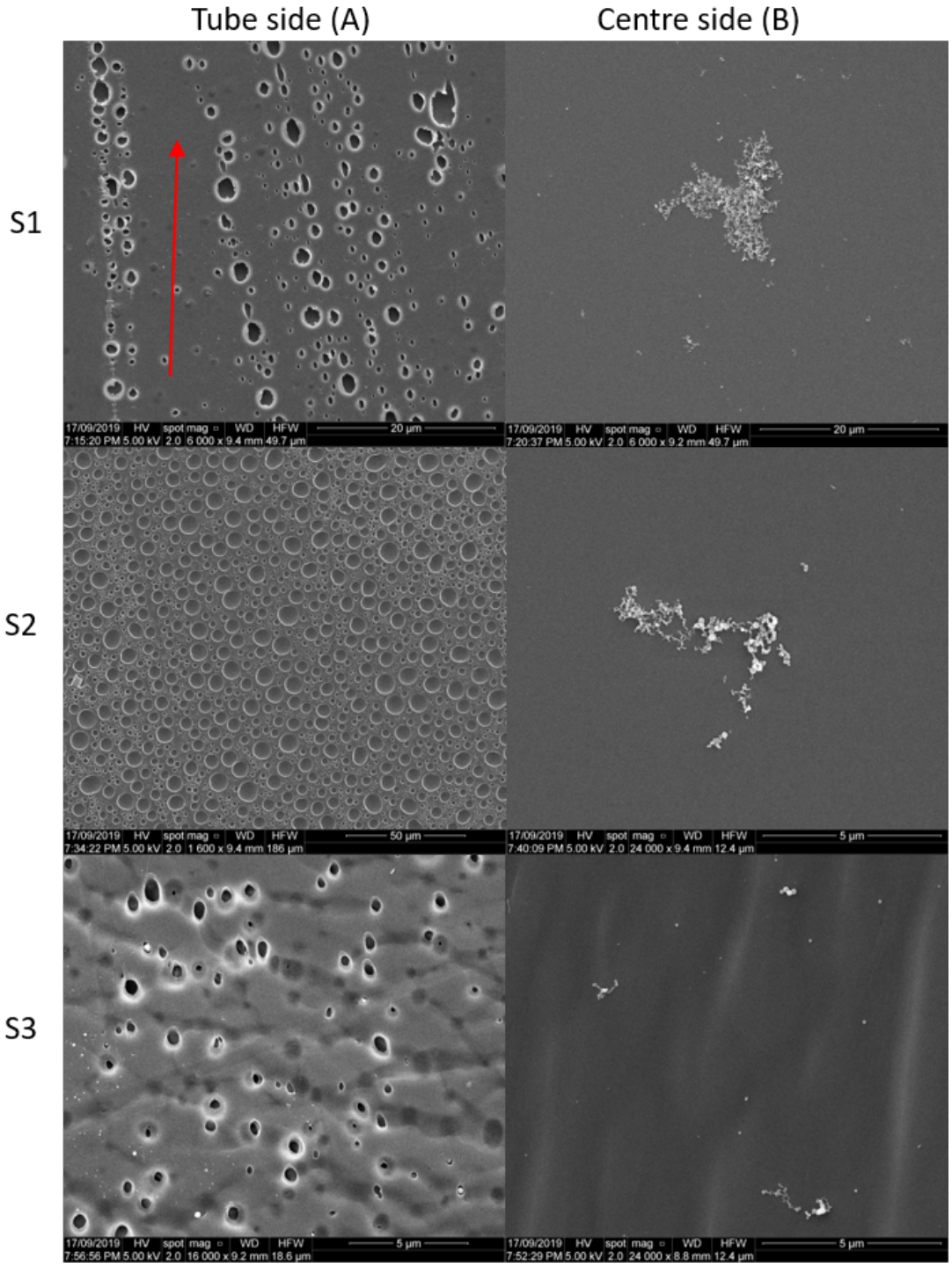

Figure S39: SEM images of S1, S2, and S3 from both sides (left: bottom of the thin film (A), right; upper side of the thin-film (B) of the thin-film processed in toluene at 7k rpm, θ = 60°, room temperature, and 30 min processing, then washed with hexane, and dried under nitrogen gas. The red arrow defines the direction of rotation of the axis of the tube, directed out of the tube.

Sample 8:

Rotational speed : 5k rpm

Tilt angle, θ : 60°

Solvent : Toluene

Time : 30 min

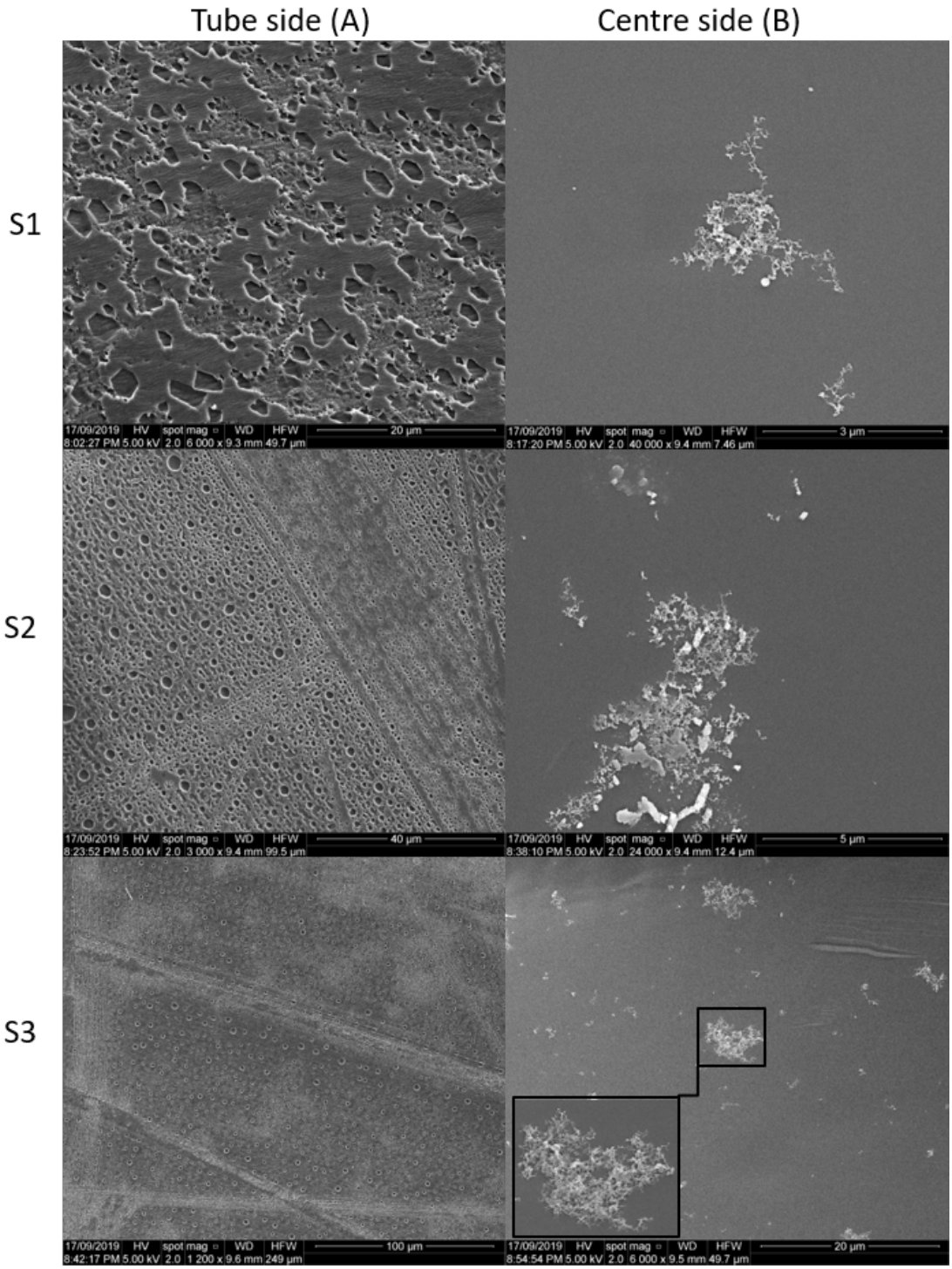

Figure S40: SEM images of S1, S2, and S3 from both sides (left: bottom of the thin film (A), right; upper side of the thin-film (B) of the thin-film processed in toluene at 5k rpm, θ = 60°, room temperature, and 30 min processing, then washed with hexane, and dried under nitrogen gas.

Sample 9:

Rotational speed : 3.5k rpm

Tilt angle, θ : 60°

Solvent : Toluene

Time : 30 min

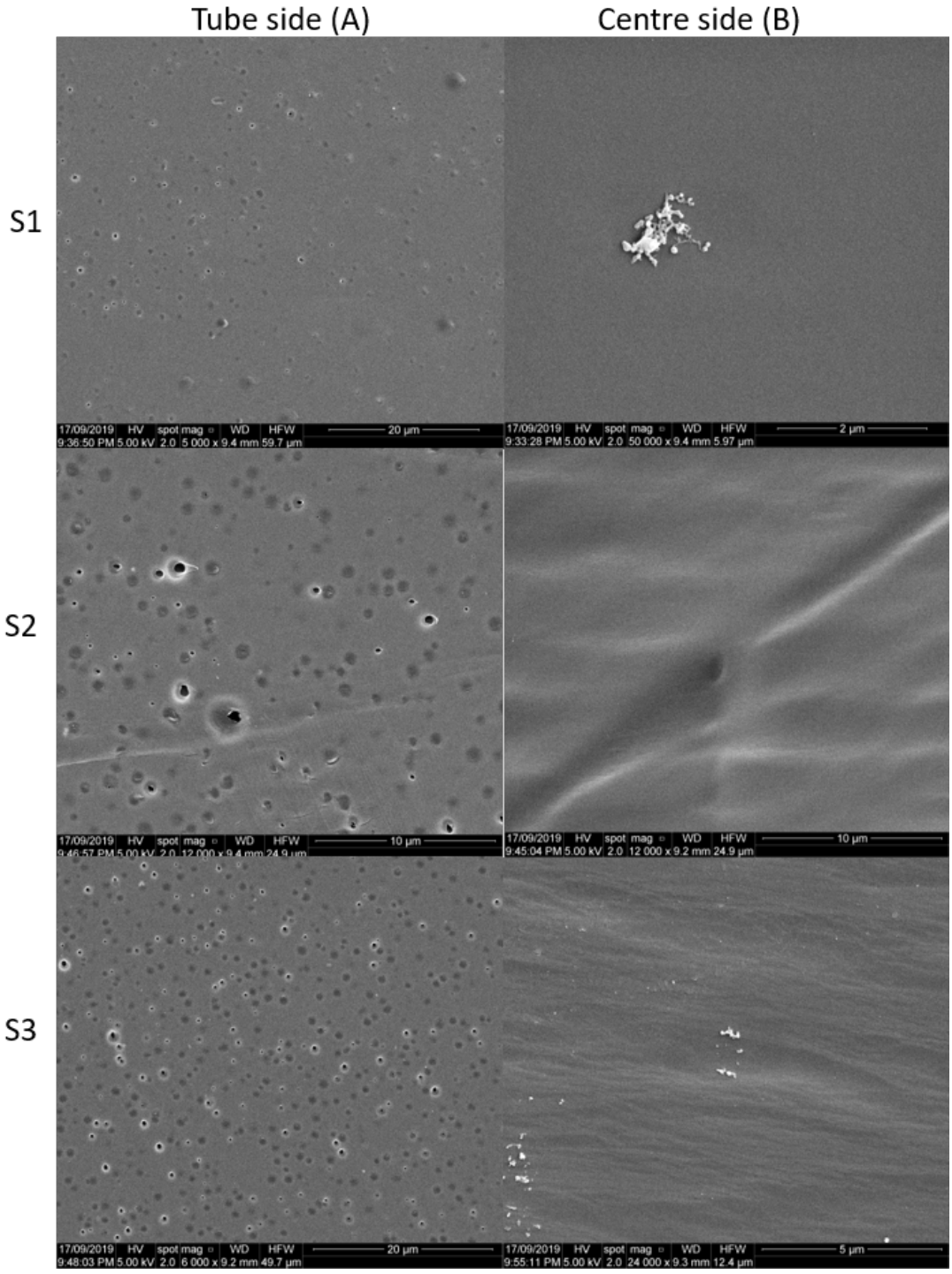

Figure S41: SEM images of S1, S2, and S3 from both sides (left: bottom of the thin film (A), right; upper side of the thin-film (B) of the thin-film processed in toluene at 3.5k rpm, θ = 60°, room temperature, and 30 min processing, then washed with hexane, and dried under nitrogen gas.

Fig. S8j-S8s show that thin-films of PSF formed in the VFD (20 mm OD, 17.5 mm ID tube) involving evaporation of a DCM solution of the polymer, have smooth surfaces, both on the surface in contact with the glass, and the surface exposed to air. Processing then with toluene in the tube reveals indentations/holes on the surface attached to the glass, with periodic regularity and alignment with the direction of rotation of the tube, for $\theta = 45^{o}$, for rotational speeds $\geq$ 5k rpm, with the indentations/holes smaller and more uniform compared with those created at 5k rpm, and for ω = 3.5k rpm the films have fewer holes, with no evidence of them being ordered. This finding for toluene is in accord with the signature for toluene, where double helical flow prevails > 6k rpm, Fig. 2. Processing of toluene solutions at $\theta = 30$ and 60^{o} also show 'molecular drilling', but these angles are not optimal for any applications of the VFD. While the upper surfaces (SB) of the films are almost devoid of holes, regions of agglomerated particles of the polymer are evident, ca 100 nm in diameter, for example in Fig. S34. These particles are likely formed during the 'molecular drilling' process, when the double helical flow strikes the surface of the tube, Fig. 1, but attempts to measure them using DLS were unsuccessful, and we then turned to using small angle neutron scattering (SANS) for further characterisation, with the findings reported below.

Real time VFD processing small angle neutron scattering (SANS)

Understanding the effect of the fluid flow in the VFD (confined mode) was explored using real time SANS. This was to determine any change in morphology of the surface of the polymer film and identify any nanoparticles of the polymer extruded from the polymer film during 'molecular drilling' (double helical flow) into the dynamic thin film of toluene.

A 20 mm OD (17.5 mm ID) VFD quartz tube containing 2 mL of toluene-d8 was rotated at 5k rpm and the scattered neutrons were counted for 2 hours in both high and low Q-range, at 1.3 and 14-meter camera length respectively. Combining both Q-range data resulted in flat curves shown in Fig. S43. The internal surface of quartz VFD tubes were then coated with a PSF thin-film at $\theta = 5$ °, ω = 6k rpm, at room temperature during 15 min (as discussed above). 5, 2 and 1 mL of toluene-d8 was then added to these tubes and individually studied using real-time SANS, for ω = 3.5k, 5k and 7k rpm, respectively, using both 1.3 and 14-meter camera lengths. Scattering for the whole Q-ranges of PSF films in the presence of toluene-d8 at these rotational speeds are plotted in Fig. S44.

The recorded scattering curves for toluene-d8 (no PSF film in the tube) are similar to scattering curves for toluene-d8 and PSF film, taking into account thinner films of toluene for high rotational speeds. The thickness of the PSF thin-film was ~ 4 μm which is out of range of SANS capabilities, as is the case for pores of the size commensurate with the morphology of the films post VFD processing, established using SEM. Importantly there was no scattering associated with nanoparticles of polymer present in solution during the processing. The presence of such particles was expected given the presence of small amounts of aggregates

of them post VFD processing, albeit only on the upper surface of the PSF film (SB), ca 100 nm in dimeter. Thus, such particles present during processing are in low concentration, beyond the level of perturbing the scattering curve for the *in situ* SANS experiments. This finding is consistent with such generated particles being constantly taken up in the polymer film, driven by the associated centrifugal force in the VFD, with the only particles present representing a snapshot of nanoparticles in equilibrium with the polymer film. Moreover, this is also consistent with the smoothing out of holes generated by the 'molecular drilling', with their presence inferred from the pocket of liquid trapped on the surface of the PSF film in contact with the surface.

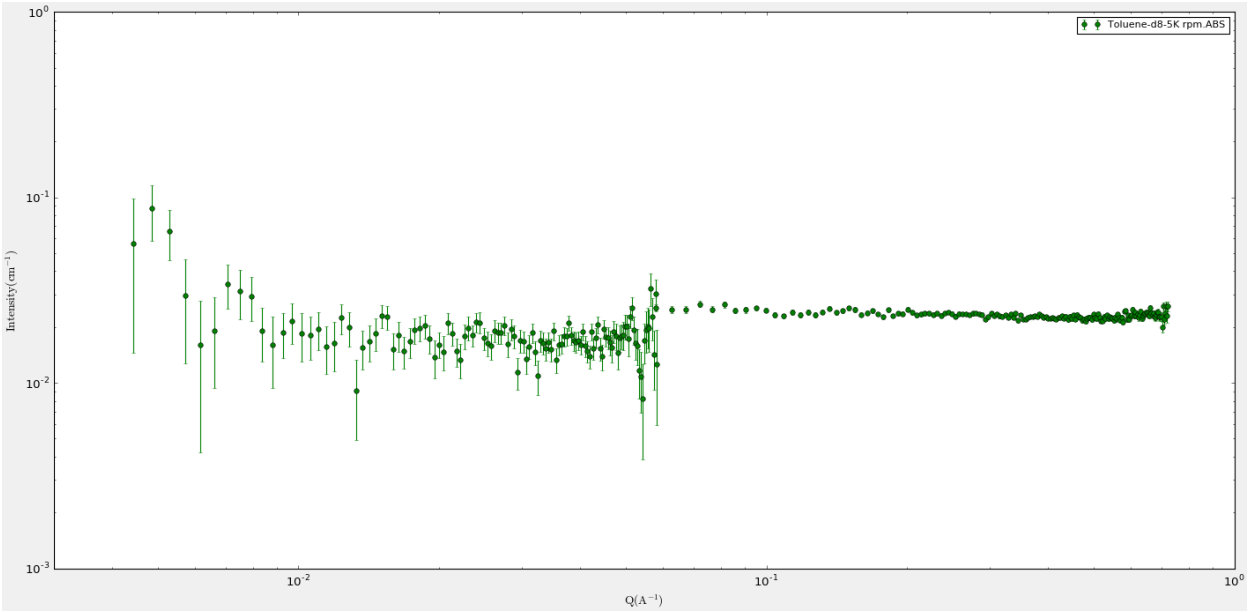

Figure S42: Real time SANS scattering in the VFD for 2 mL of toluene-d8 in a 20 mm OD quartz tube (no PSF coating) rotated at 5k rpm for 2 hours, at room temperature, θ = 45°.

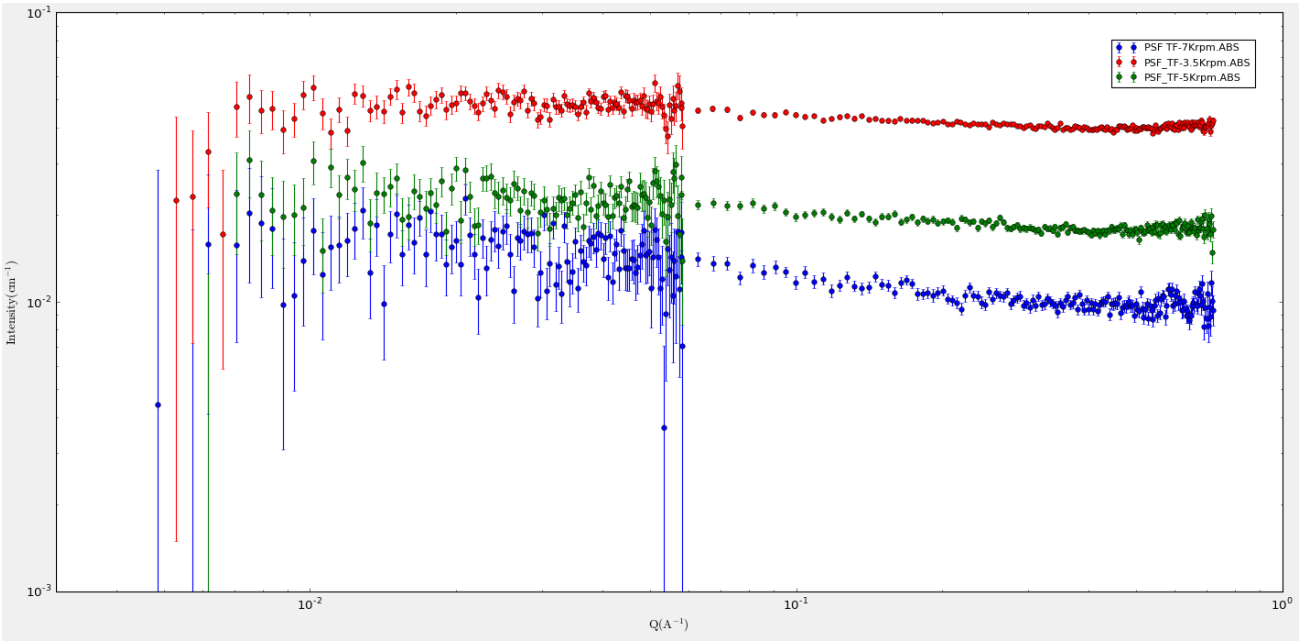

Figure S43: Real time SANS scattering in the VFD for toluene-d8 in a PSF coated 20 mm OD quartz rotated at 3.5k, 5k and 7k rpm (using 5, 2 and 1 mL of toluene-d8, respectively), for 2 hours at room temperature, $\theta = 45°$.

9. BSA polymerisation with glutaraldehyde

The process for fabricating macroporous spheroidal particles using the VFD involved adding specific volumes of ethanol solution to a specified volume of BSA using the de-solvation method at 1 mg/mL at room temperature as a slightly modified published process[3]. As shown in Fig. S45, in a 'standard' VFD (20 mm OD, 17.5 mm ID, length 18.9 cm), volume combinations for BSA (1 mg/mL in 10 mM PBS), ethanol, and glutaraldehyde were 300, 900, and 15 µL, respectively. Then, 1 mL of a combined solution was quickly transferred to the VFD and the glass tube was spun at 3k, 5k, 6k, 7k or 9k rpm for 1 min. For the VFD housing a 'small' VFD tube (10 mm OD, 8.5 mm ID, length 19.9 cm), volume combinations for BSA (1 mg/mL in 10 mM PBS), ethanol, and glutaraldehyde were the same as for 20 mm OD VFD tube. Then, 0.5 mL of the combined solutions was quickly transferred to the 10 mm tube which was spun at 3k, 5k, 6k, 7k or 9k rpm for 1 min. Post VFD processing, samples were recovered by centrifugation at 11800 g for 15 min and washed with the same volume of MilliQ water three times to remove excess reactants.

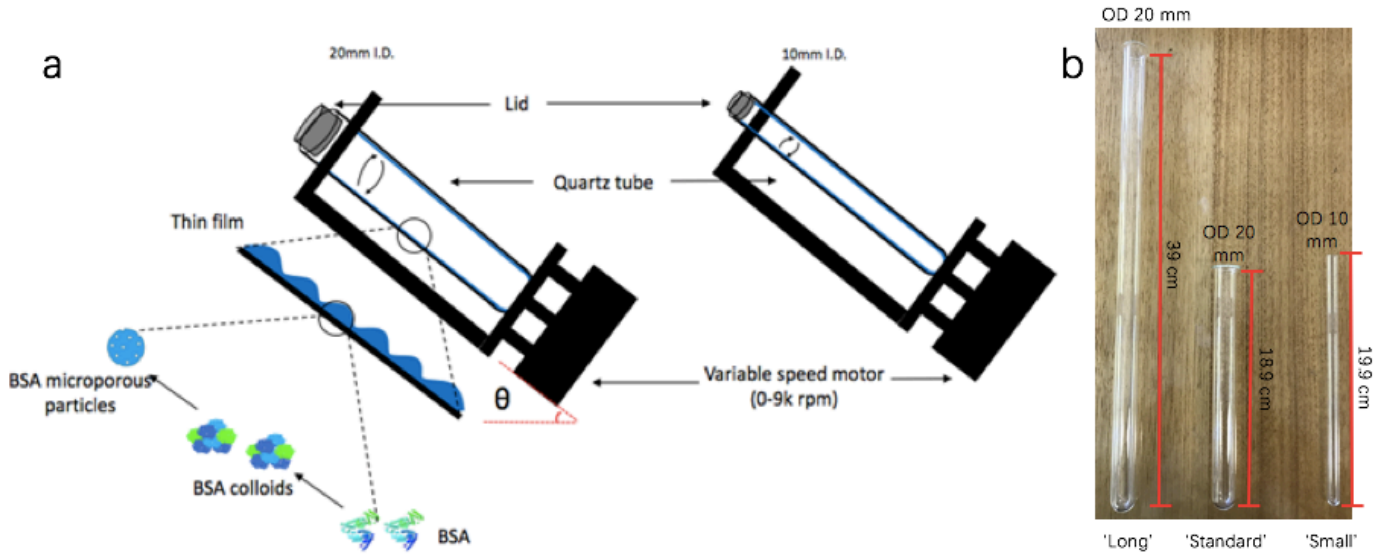

Figure S44: (a) Schematic of the preparation of BSA nanoparticles in a standard VFD (20 mm OD, 17.5 mm ID) and a VFD (10 mm OD, 8.5 mm ID) operated under confined mode of operation, at θ = 45°. (b) Photo of the VFD tubes in three different dimensions labelled as 'Long' for a long VFD tube (20 mm OD, 17.1 mm ID, 39 cm length), 'standard' for a standard length VFD tube (20 mm OD, 17.5 mm ID, 18.9 cm length) and 'Small' for a small diameter VFD tube (10 mm OD, 8.5 mm ID, 19.9 cm length).

Reaction of BSA with glutaraldehyde in the VFD in a 3:1 mixture of ethanol and PBS (10 mM dissolved in MilliQ water) results in polymeric spheres with inbuilt porosity[3]. Synthesis of homogeneous spheroidal BSA nanoparticles applies to both 10 mm and 20 mm VFD for all the explored rotational speeds, 3k, 5k, 6k, 7k and 9k (Figure 4 and Figure S46). The average size of the spheres fluctuates slightly from 3k to 9k in both 10 mm and 20 mm OD VFD tubes (Fig. S47). The size of the porous spheres is *ca*. 10-38% less for the 10 mm OD

tube relative to the 20 mm tube, except at 3k rpm (Fig. S46(a)). Particle size [dynamic light scattering (DLS)] was determined using a Malvern particle size analyzer (Malvern Zetasizer). The results for material prepared in a 'standard' 20 mm OD and 'small' 10 mm OD VFD tube are compared with results obtained previously using a 'long' VFD tube[3] (diameter *ca.* 358 to 600 nm), with the particles prepared in the 'standard' and 'short' tubes less monodispersed in solution (Fig. S9c(b)) compared to those prepared in the long VFD tube[3]. Agglomeration was observed when samples were dispersed in MilliQ water. On the other hand, VFD generated macroporous BSA nanoparticles are always more uniform in size relative to using conventional benchtop vortex mixing (0.5 mL or 1 mL) (Fig. S47(b,c)), affording spheres with less inbuilt porosities, no inbuilt porosities and irregular microsized structures (Figure S48(a,b)). The results are consistent with the DLS (Figure S47(c)) and previously published result[3].

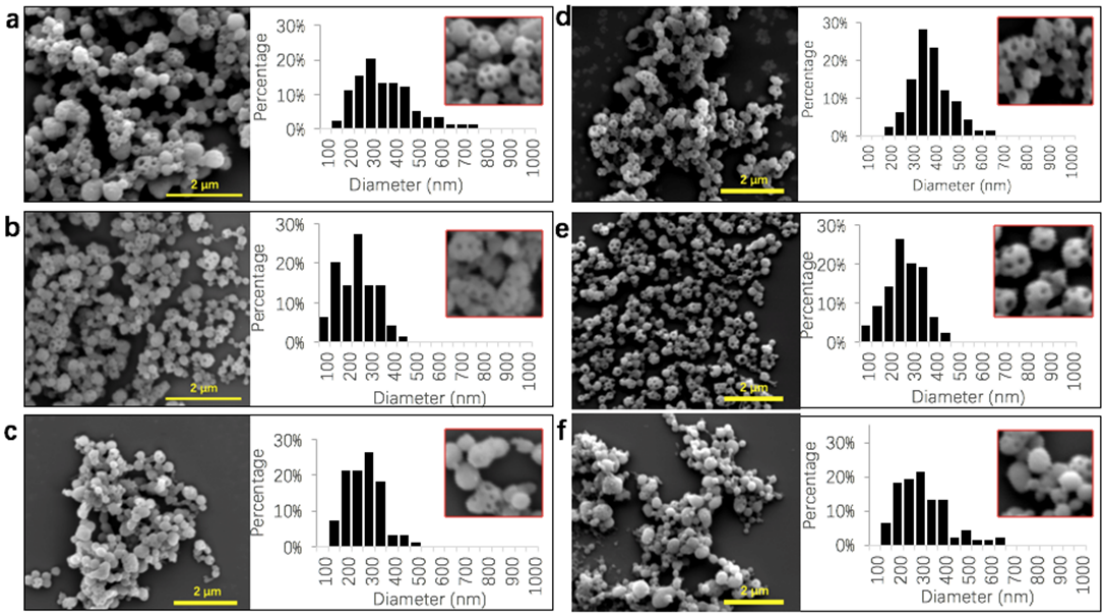

Figure S45: SEM images of BSA nanoparticles fabricated in the VFD for 1 min with BSA (1 mg/mLin 10 mM PBS), ethanol and glutaraldehyde of 300 µL, 900 µL and 15 µL, respectively. 0.5 mL of combined solution in a 10 mm OD tube at 3k, 6k and 9k rpm (a) – (c) respectively, and 1 mL of combined solution for a 20 mm OD tube, at 3k, 6k and 9k rpm (d) – (f) respectively, reporting SEM images and derived particle size distributions from 100 randomly chosen spheres.

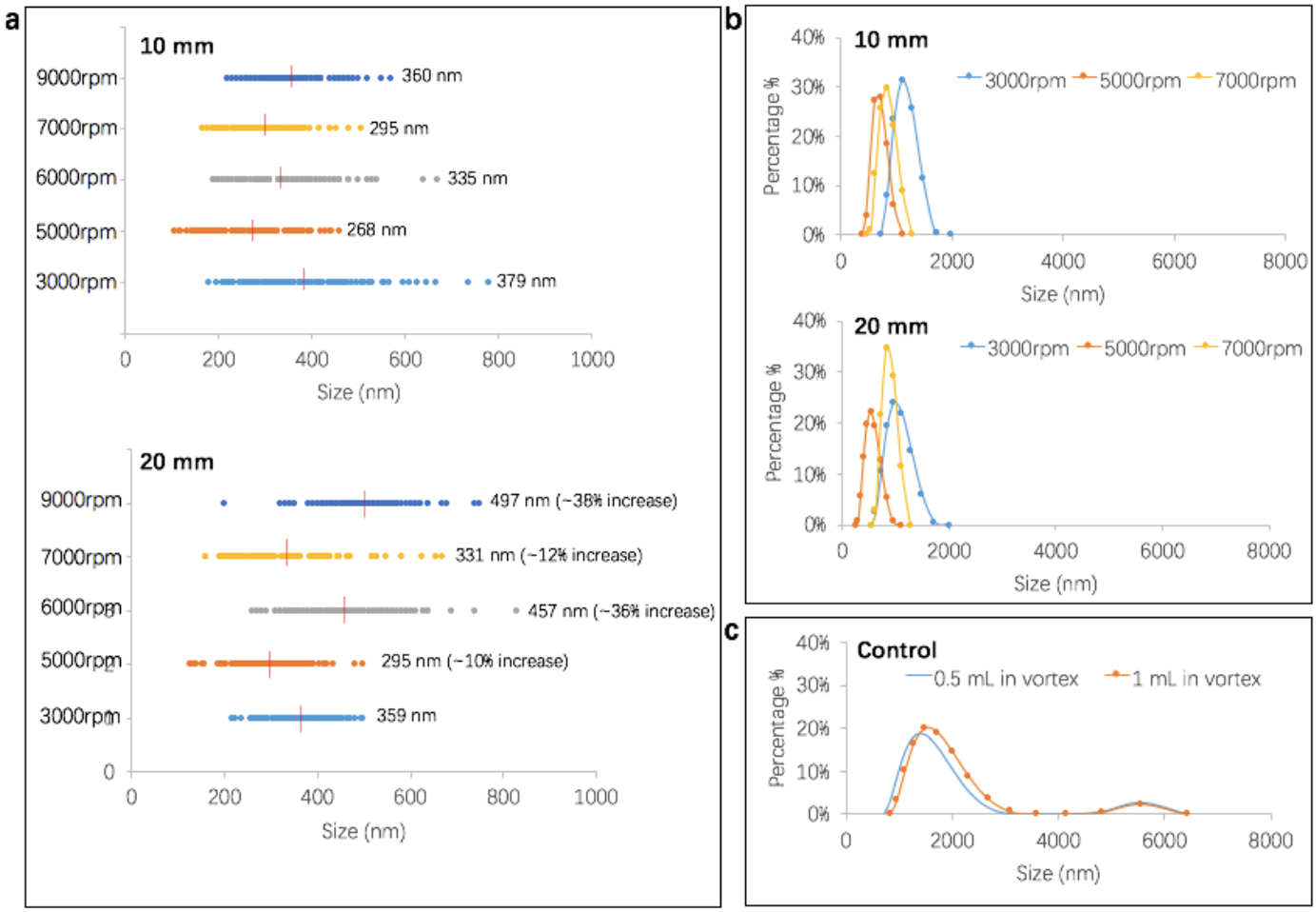

Figure S46: (a) Size distribution of BSA nanoparticles (based on SEM) prepared in 10 and 20 mm OD VFD tubes rotating at 3k, 5k, 6k, 7k or 9k rpm, respectively. The average sizes of the particles are shown behind each condition, with the percentage of size increment for a 20 mm OD VFD tube shown in brackets relative to those prepared in a 10 mm OD VFD tube, and highlighted as red dash lines. (b) DLS of BSA nanoparticles prepared in 10 and 20 mm OD VFD tubes (c) DLS of BSA nanoparticles prepared using bench-top vortex. Controls were prepared in two volume combinations, in either 0.5 mL or 1.0 mL, which is equivalent to VFD processing.

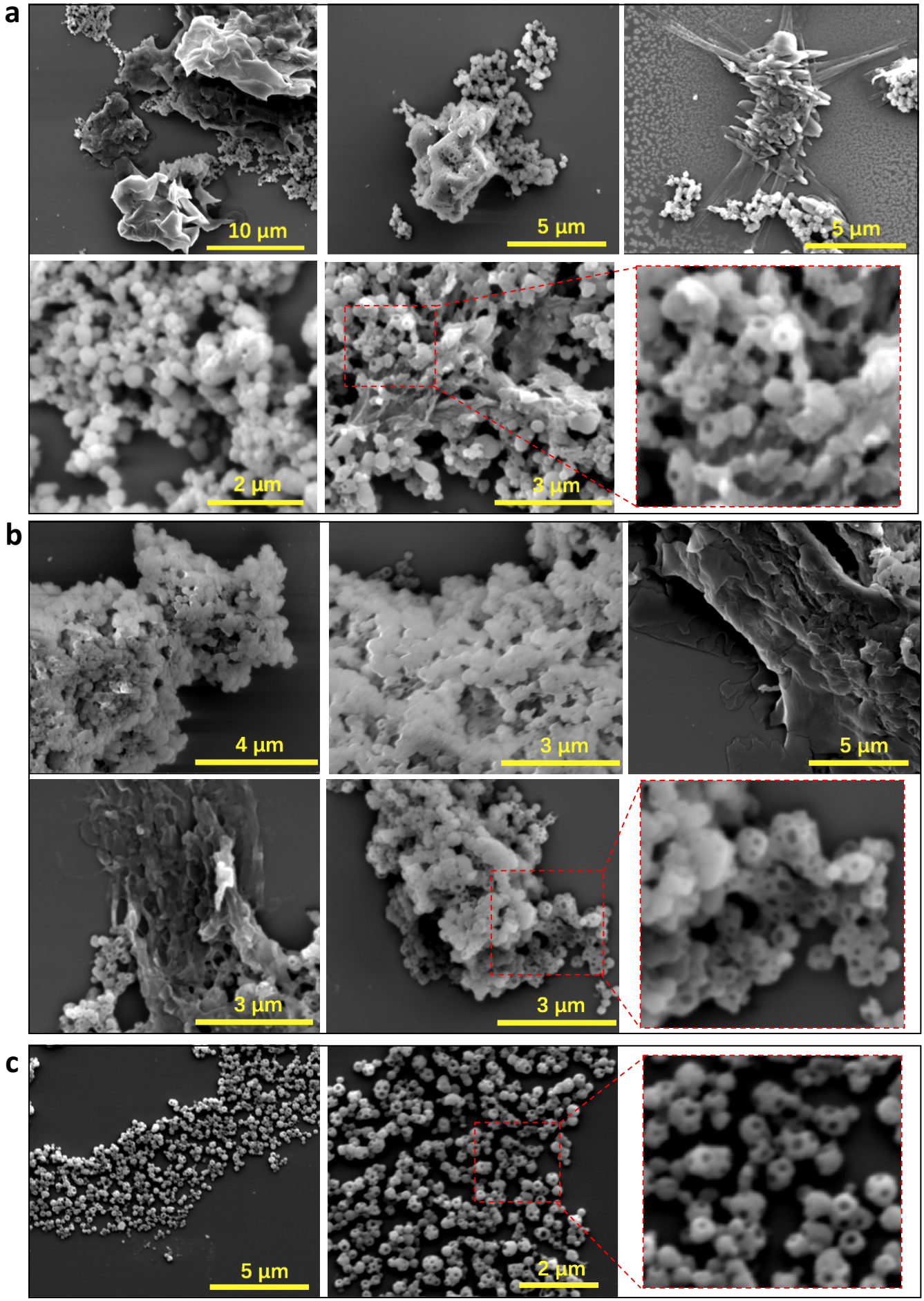
a
10 µm
5 µm
5 µm
2 µm
3 µm
b
4 µm
3 µm
5 µm
3 µm
3 µm
c
5 µm
2 µm

Figure S47: SEM images of the BSA nanoparticles fabricated for 1 min from BSA (1 mg/mL in 10 mM PBS), ethanol and glutaraldehyde, for 300, 900 and 15 µL, respectively (a) and (b) SEM of material formed in 0.5 mL or 1 mL respectively, of combined solution using a bench-top vortex, compared to (c) using 1 mL of combined solution in a 20 mm OD VFD tube rotating at 5k rpm.

10. MOF-5 fabrication

Conventional nano-molding technology (NMT) or injection moulding is a method of producing polymeric products of all shapes and sizes with nanoscale dimensions[4]. Different from conventional NMT, the fluid flow in the VFD is used to fabricate micron/sub-micron particle, as new concept in nano-moulding. To mould the liquid of flow, several material systems were utilized. Porous metal organic frameworks (MOFs) feature in the VFD moulding experiments, focusing on MOF-5 or $Zn_4O(BDC)_3$ which normally forms crystals with cubic morphology[5].

The fabrication of MOF-5 using VFD was conducted as previously published method with modifications[6]. A solution of $Zn(OAc)_2 \cdot 2H_2O$ (85.2 mM), H_2BDC (33.56 mM) and TEA (67.13 mM) in 1 mL DMF was prepared and allowed to react in the VFD. Briefly, H_2BDC (63.3 mg) and TEA (106.3 µL) were dissolved in 4.894 mL of DMF. $Zn(OAc)_2 \cdot 2H_2O$ (169.9 mg) was dissolved in 5 mL of DMF. For a typical VFD experiment, 556 µL of zinc solution was added to 444 µL H_2BDC followed by 20 mm VFD processing for 30 min at a temperature as indicated. The synthesis of MOF-5 involving VFD processing is based on the observation of phase purity and crystal morphology, using XRD and SEM. Post-VFD processing at 110ºC there was some material adhering to the surface of the tube ($MOF_{surface}$) with the rest falling to the bottom of the tube (MOF_{tube}) (Fig. S49). In this case, the two samples were separately collected and mounted on silicon wafer for SEM imaging. To minimise exposure to humid air, silicon wafers with mounted samples were quickly dried in oven at 110ºC, followed immediately by SEM imaging.

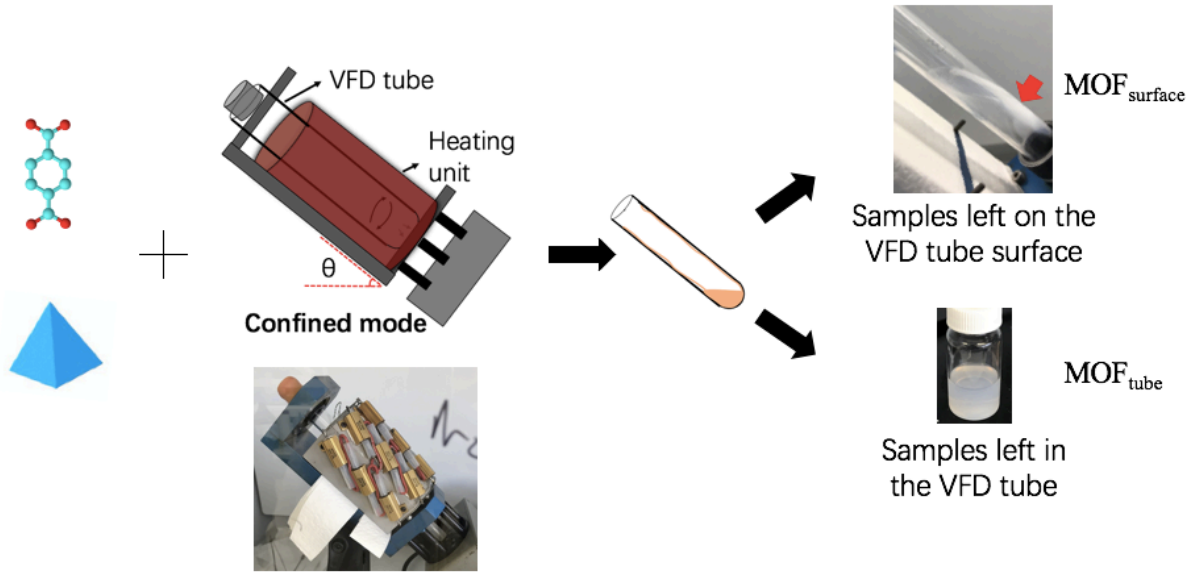

Figure S48: Schematic of the synthesis of MOF5. H_2BDC (63.3 mg) and triethylamine (106.3 µL) were dissolved in 4.894 mL of DMF. $Zn(OAc)_2 \cdot 2H_2O$ (169.9 mg) was dissolved in 5 mL of DMF. For a typical VFD experiment, 556 µL of zinc solution was added to 444 µL H_2BDC followed by VFD processing in a 20 mm OD tube for 30 min at 110ºC. Post-VFD processing, $MOF_{surface}$ material was separated from MOF_{tube} material collected at the bottom of the tube.

MOF-5 is commonly prepared using solvothermal method by heating a mixture of H_2BDC and zinc nitrate[6]. However, this involves long processing times, hours to weeks[7]. Tranchemontagne *et al.* reported a method of preparing MOF-5 at ambient temperature over 2.5 h using zinc acetate[5]. Subsequent addition of triethylamine resulted in deprotonation of the H_2BDC and precipitation of MOF-5. This result led to adapting the reaction for the growth of MOF-5 crystals using VFD processing.

To minimise errors associated with exposure to air, sample preparation was first optimised for characterisation using SEM, noting that the morphology of MOF-5 is affected by exposing to water or humid air (Fig. S50(a,b)), in agreement with previous findings[8]. In addition, any residual solvent needs to be rapidly removed post processing, for reproducible purposes (Fig. S50(c)). Therefore, samples were centrifuged at 2350 g for 15 min post VFD processing to separate from the solvent, with the material then mounted on a silicon wafer and carefully dried at the same temperature as that used in VFD processing. VFD processing at 22ºC induces the formation of nanoscale MOF seeds with spherical shape, for all speeds from 3k to 7k rpm, after a reaction time of 30 min (Fig. S51), which showed no significant difference relative to the control experiment conducted without VFD. Increasing the temperature to 60 and 110ºC resulted in cubic crystals, which was barely observed for the control (Fig. S52 and S53). XRD of the material formed in the VFD established that they are MOF-5 by comparing with the pattern simulation from the EVA database (Fig. S54). Operating the processing

in the VFD at either 60 or 110ºC had no effect on the phase composition after 30 min of processing, all in a 20 mm OD tube, with θ at 45º.

It was noted that at 110ºC, white materials appeared along the VFD tube surface (named as $MOF_{surface}$) and these were automatically separated from the samples collected from the bottom of the tube (named as MOF_{tube}) after stopping the VFD (Fig. S49). $MOF_{surface}$ samples were dominated by porous surfaces, especially at 3, 4 and 5k rpm. Above 5k rpm, the particles have flat surfaces (Fig. 4f). Time dependent study for 15, 30 and 60 min VFD processing at 4k rpm, 110ºC all revealed porous crystal surfaces (Fig. S55).

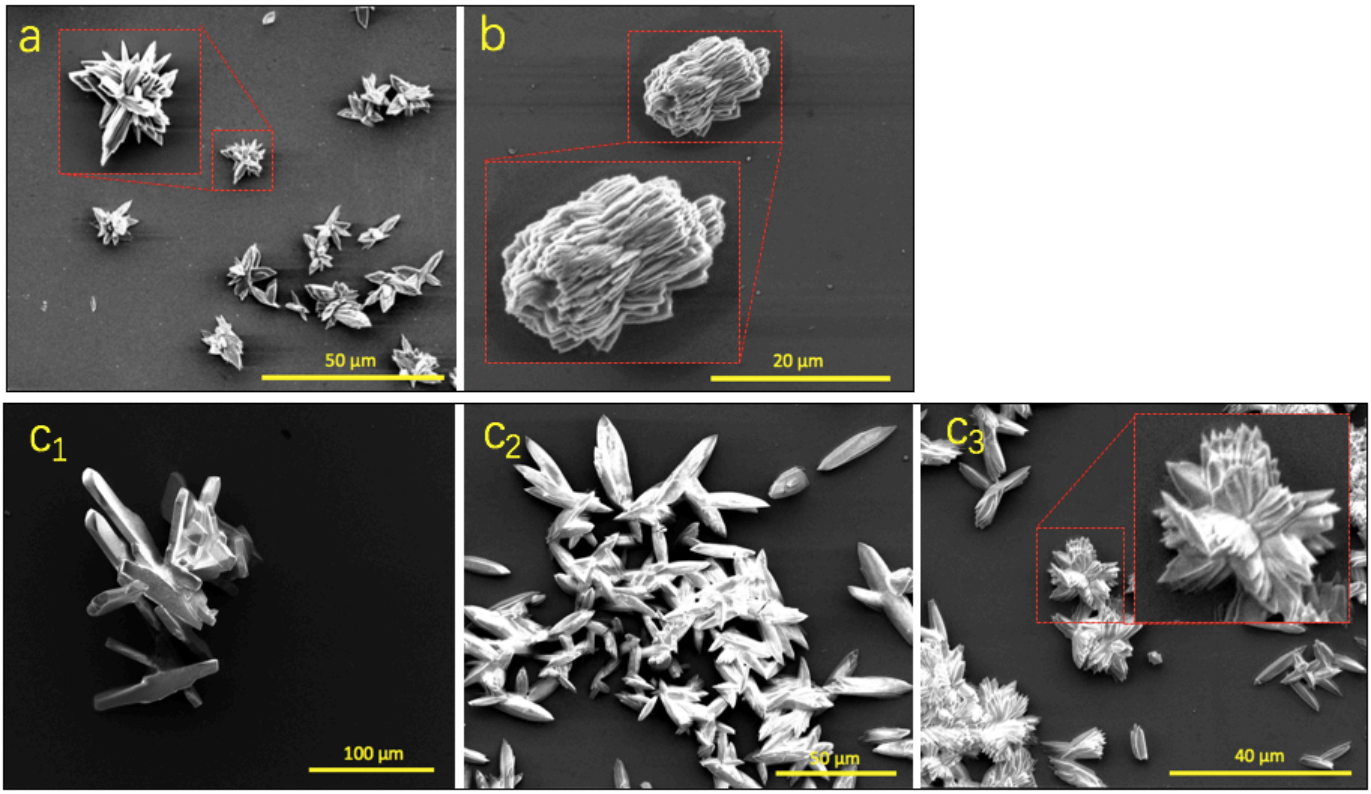

Figure S49: SEM images of MOF-5, prepared in the VFD at 4k rpm for 30 min. (a) Post VFD processed material, where the sample for SEM was prepared by quickly diluting the solution *ca* 200 times in water, then drop cast on a clean silicon wafer and air dried. (b) As for (a) but with the dilution in DMF, (c) Post VFD processed material, where samples were directly drop cast on a clean silicon wafer without centrifugation and air dried; C_1-C_3 show SEM images from three independent experiments.

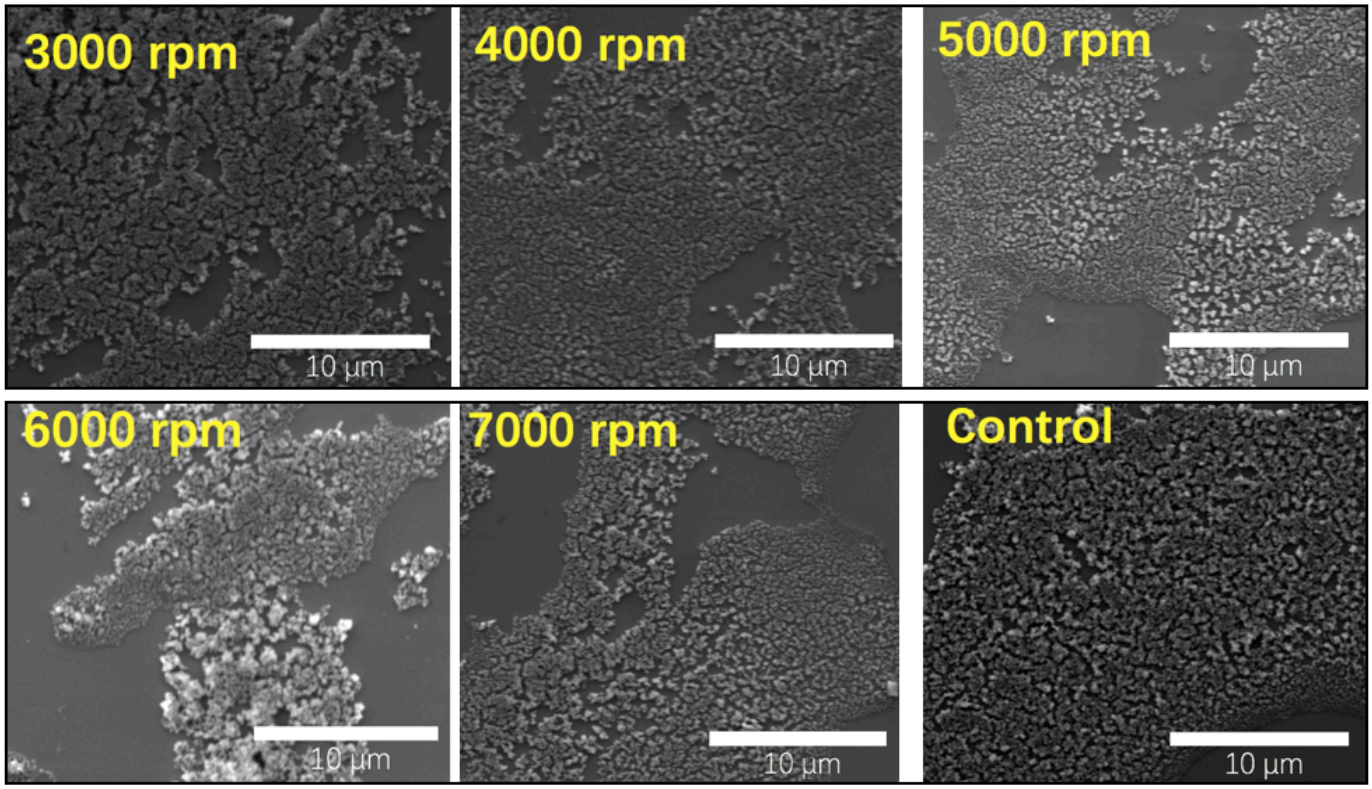

Figure S50: SEM images of material formed in 1 mL DMF solution of $Zn(OAc)_2 \cdot 2H_2O$ (85.2 mM), H_2BDC (33.56 mM) and TEA (67.13 mM). VFD processing at 22ºC for 30 min, 20 mm OD tube, θ = 45º, for different rotational speeds relative to the control experiment carried out at the same temperature, no VFD. Post processing, MOF_{tube} samples (as specified in Fig. S10a) were centrifuged at 2350 g for 15 min with some of the collected pellet drop cast on a silicon wafer and dried at 22ºC prior to SEM characterisation.

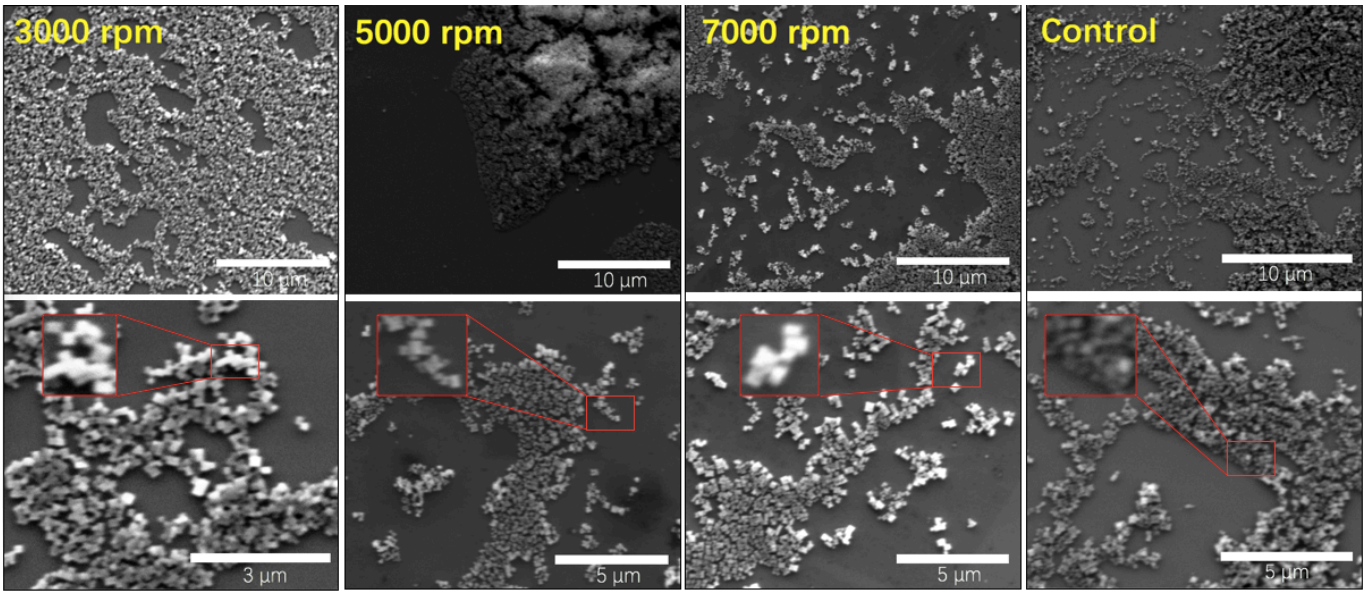

Figure S51: SEM images of material prepared in a 1mL DMF solution of $Zn(OAc)_2 \cdot 2H_2O$ (85.2 mM), H_2BDC (33.56 mM) and TEA (67.13 mM). VFD processing at 60ºC for 30 min, 20 mm OD tube, θ = 45º, for different rotational speeds relative to the control experiment carried out at the same temperature, no VFD. Post

processing, MOF_{tube} samples (as specified in Fig.S10) were centrifuged at 2350 g for 15 min, with some of the collected pellet drop cast on a silicon wafer and dried at 60ºC prior to SEM characterisation.

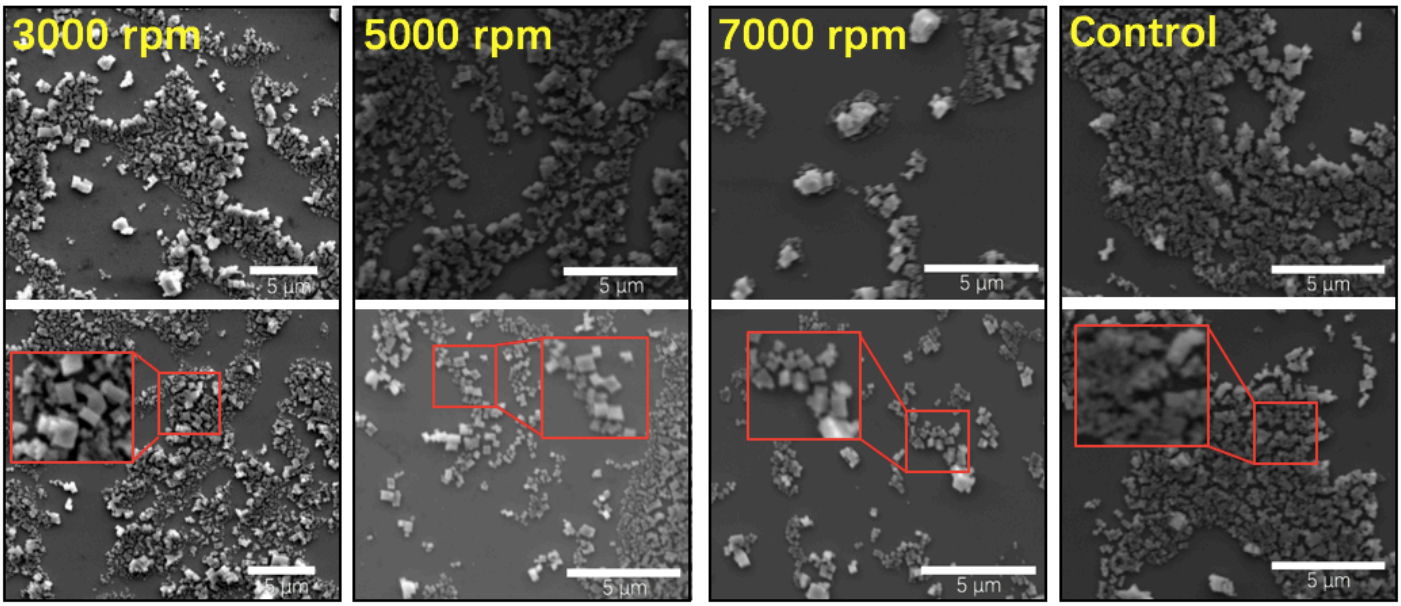

Figure S52: SEM image of material prepared in a 1 mL DMF solution of $Zn(OAc)_2 \cdot 2H_2O$ (85.2 mM), H_2BDC (33.56 mM) and TEA (67.13 mM). VFD processing at 110ºC for 30 min, 20 mm OD tube, $\theta = 45^o$, for different rotational speeds relative to the control experiment carried out at the same temperature, no VFD. Post processing, MOF_{tube} samples (as specified in Fig.S10) were centrifuged at 2350 g for 15 min, with some of the collected pellet drop cast on a silicon wafer and dried at 110ºC before SEM characterisation.

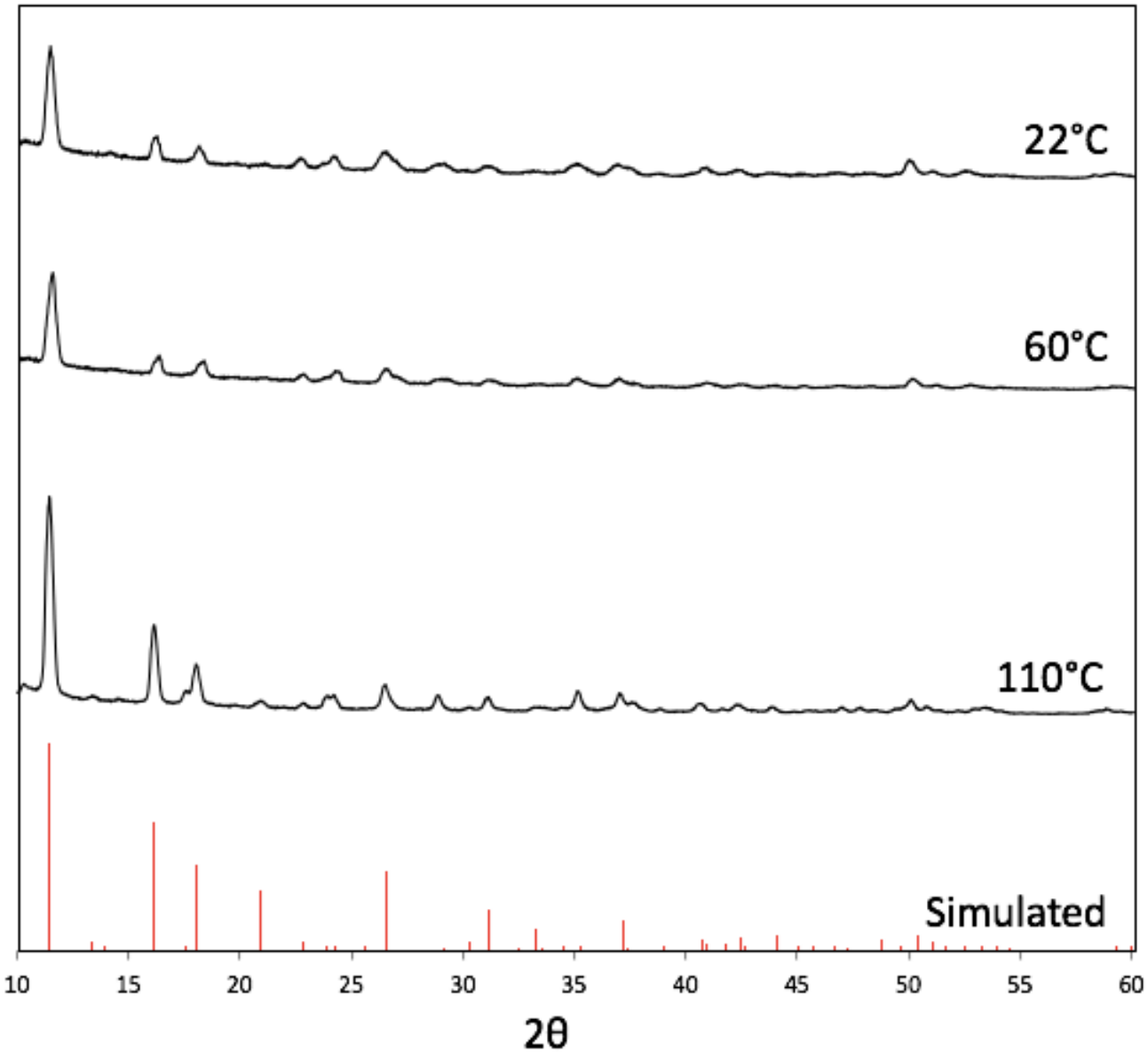

Figure S53: XRD pattern of MOF-5 prepared using VFD (MOF_{tube}), formed at ω = 5k rpm for 30 min at 22, 60 or 110ºC, respectively, θ = 45º, for a 20 mm OD tube, along with the simulated pattern for the MOF derived from the EVA database.

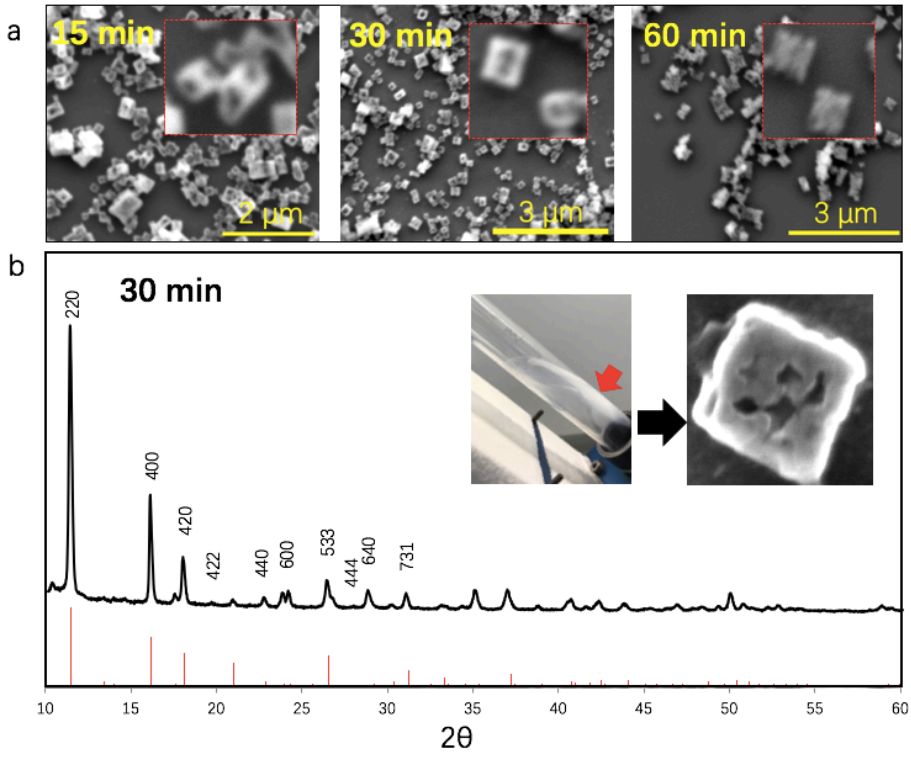

Figure S54: (a) A solution of $Zn(OAc)_2 \cdot 2H_2O$ (85.2 mM), H_2BDC (33.56 mM) and TEA (67.13 mM) in 1 mL DMF was prepared and processed in the VFD (confined mode, 20 mm OD tube) at 110ºC for 15 min, 30 min and 1 h, ω = 4k rpm, θ = 45º, with the resulting $MOF_{surface}$ sample characterised using SEM. (b) XRD pattern of MOF-5 ($MOF_{surface}$) formed after 30 min at 110ºC and the simulated structure derived from the EVA database.

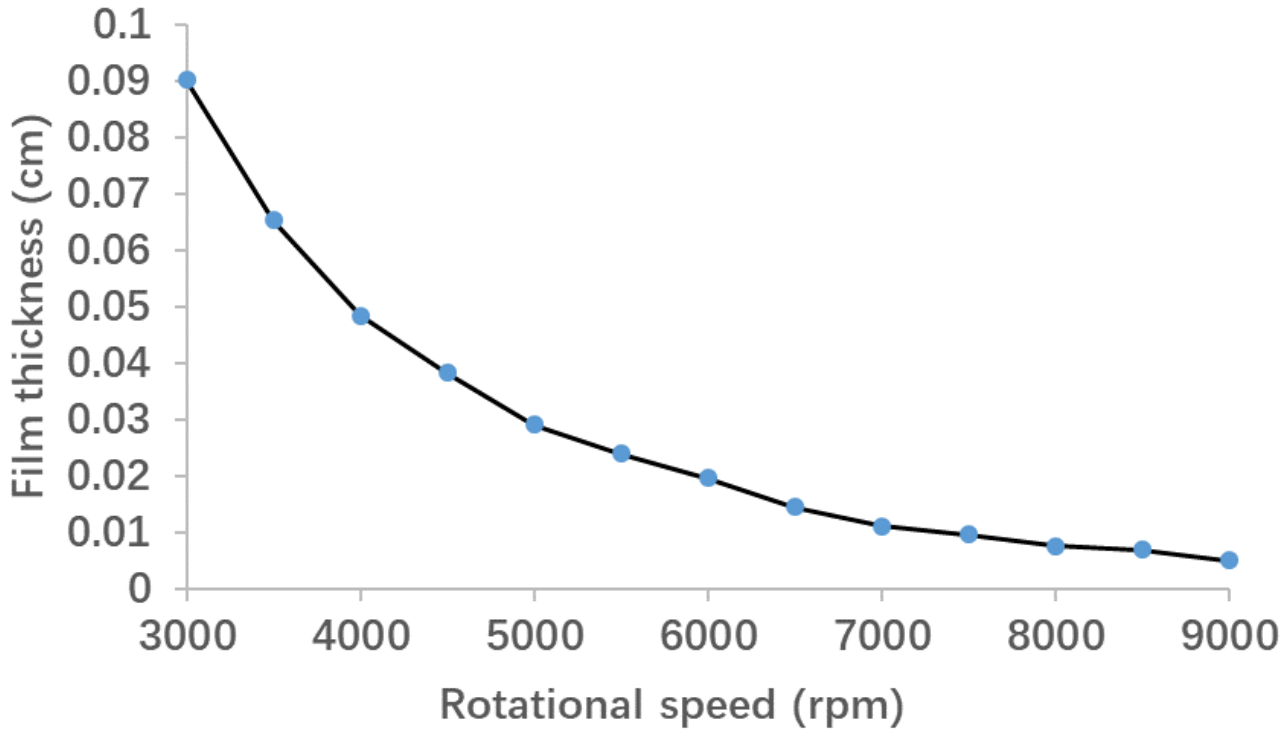

Figure S55: The change in film thickness, *d*, for DMF as a function of rotational speed, ω, at 110ºC in a 20 mm OD tubes, at θ = 45º. This is derived from measuring the volume of the liquid in the tube at each speed, where the liquid is to the top of the tube while being spun at a particular ω, with each data point repeated in triplicates. The experimental set up with a heating block over the rotating glass tube, circumvented determining the other signature characteristics of DMF at 110ºC, namely any increasing in temperature and effects on mixing as ω increases.

11. Fluid Dynamics within the Vortex Fluidic Device

In order to further explain the fluid dynamics within the VFD, computational fluid dynamics (CFD) simulations have been conducted using the OpenFoam v1806[9]. In order to build a practical simulation to investigate the fluid dynamics within the VFD, a thin-cross section of the VFD tube perpendicular to the axis of rotation was modelled. The CFD simulation was reduced into 2D by considering a thin slab, *d*=100 nm (1 cell thickness). This meshing of the cylindrical slab in the *xy*-plane was divided in two regions (see Fig. S57). Here we have a high resolution mesh region (Region 1, 100 x 100 cells) and a low resolution mesh region (Region 2, 100 x 100 Cells). Region 2 describes the internal volume of the cylinder, with radius 8.3 mm, while region 2 describes the volume outside of Region 1 to the internal test tube wall, r = 8.75 mm. The high resolution mesh at the outermost radii was required in order to describe the thin liquid film located on the test tube wall. The outside wall of Region 1 provided a rotational wall boundary condition about the VFDs axis of rotation (*z*-axis). Here the rotational wall velocity, ω, corresponds to the rotational speed of the VFD tube. The interFoam solver was select to perform the simulations. This solver implements a volume of fluid (VOF) phase-fraction based approach to solve the continuity, phase-fraction transport, and momentum equations. Here the alpha phase fraction, proportions a cell between the liquid (water or toluene, α=1) and gas (air, α=0) phase fractions.

The simulation was run using a fixed volume of fluid method, initiated by filling the outermost cylindrical section with fluid (α = 1) for radii, r >8.55 mm (giving a uniform thickness liquid layer of 200 µm). The calculation was implemented using α = 1 and constant pressure boundary conditions on the inner tube wall.

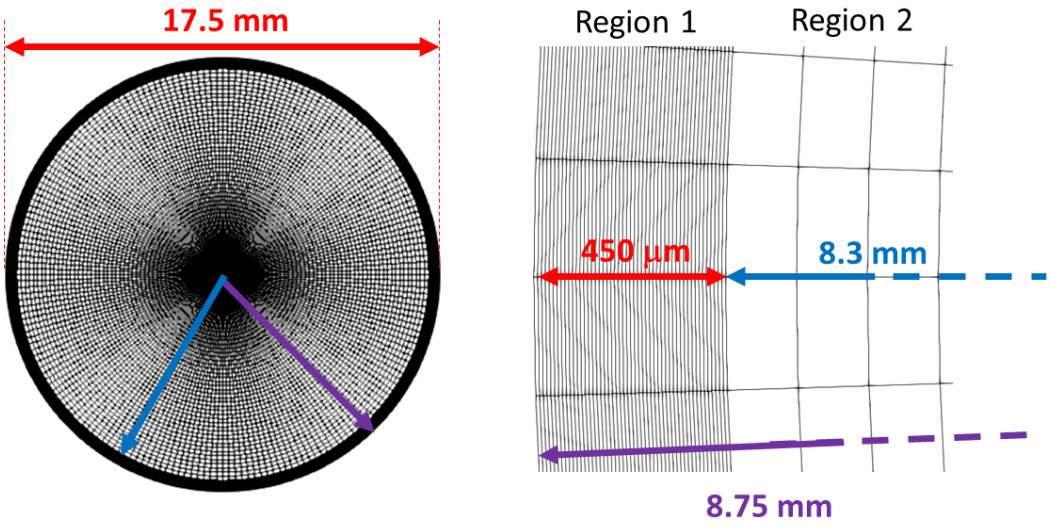

Figure S56: The mesh of the VFD tube used for the CFD simulations.

In analysing the results, the relative flow velocity ($\boldsymbol{u}_r$) (in the rotating frame of reference) is first considered;

$$\boldsymbol{u}_r = \boldsymbol{u} - \boldsymbol{\omega} \times \boldsymbol{r}$$

Here $\boldsymbol{u}$ is the calculated fluid velocity (m/s) in the inertial reference frame, $\boldsymbol{\omega}$ is the angular velocity vector (rad/s) and $\boldsymbol{r}$ is the radial vector from the axis of rotation (m). Note that the relative velocity is important, as it is responsible for the introduction of Coriolis effects through the creation of the Coriolis force per unit mass in the rotating frame, where

$$\boldsymbol{F_{Cor}} = -2\boldsymbol{\omega} \times \boldsymbol{u}_r$$

Results from the CFD simulations are presented in Fig. S11b-d and Fig. S11e-g for water and toluene at 3000, 6000 and 9000 rpm, respectively.

At low rotational speed (3000 rpm), the relative velocity, $\boldsymbol{u}_r$, oscillates between being parallel and antiparallel to the rotational direction. Here the orientation is parallel (anti-parallel) at the bottom (top) of tube with reference to the gravitational projection. This is likely to induce the Coriolis-driven circular flows, with the strength of the relative velocity component increasing in going from the tube wall towards the fluid-air interface. Note that as the viscosity of the fluid increases, the relative velocity will decrease in magnitude, lessening the importance of the Coriolis forces (as in a 3:1 ethanol/water mixture), and hence circular flows.

As the rotational speed increases to 6000 rpm, these effects remain, but the magnitude of the relative velocity is decreasing. This will manifest as a reduced influence of the Coriolis force on the fluid flow, which is consistent with the dominance of double helical flow at high ω. Note further that as the rotational period of the fluid decreases, the time/lengths scales over which the Coriolis forces are able to act decreases.

As the rotational speed is increased to 9000 rpm, the relative velocity, $\boldsymbol{u}_r$, is always anti-parallel to the rotational direction. In this case, the Coriolis force is always directed radially outwards. As such we expect that there is a fluid movement along the tube axis.

The Reynolds number of the fluid flow[10],

$$Re = \frac{uD}{\nu}$$

Where $D = \frac{4A}{p}$ is the hydraulic diameter with A being the cross sectional area of the flow, and p being the wetted perimeter. In our case, this characteristic length (D) becomes four times the film thickness, t. Note that the film thickness depends on the fluid volume in the tube, and the rotational speed. The film thickness also varies along the tube axis. For the purpose of the analysis, the average film thickness is set at 200 μm, to be consistent with our simulations. The calculated Reynolds number for both water and toluene are contained in

Table S2. Here we observe that at the lowest rotational speeds, the flow should be laminar. With the increasing rotational speed, a transitional flow region ($Re > 2000$) prevails, although as Re <10000 it is not expected that the axial flow can develop into a fully turbulent flow regime.

Table S2: Summary of rotational parameters in the VFD. The Reynolds numbers (Re) are calculated using the Wall velocity, the film thickness of 200 μm and the transport properties detailed in Table S11b.

Rotational Speed (rpm)	ω (rad/s)	f (s^{-1})	Period, T (ms)	Wall Velocity, $\|U\|$ (m/s)	*Re* (Water)	*Re* (Tol.)
1000	104.72	16.7	60.00	0.916	733	1078
2000	209.44	33.3	30.00	1.833	1466	2156
3000	314.16	50.0	20.00	2.749	2199	3234
4000	418.88	66.7	15.00	3.665	2932	4312
5000	523.60	83.3	12.00	4.582	3665	5390
6000	628.32	100.0	10.00	5.498	4398	6468
7000	733.04	116.7	8.57	6.414	5131	7546
8000	837.76	133.3	7.50	7.330	5864	8624
9000	942.48	150.0	6.67	8.247	6597	9702

Table S3: Transport properties used in the simulations.

Phase	kinematic viscosity (ν) (m^2/s)	Density (ρ) (kg/m^3)	Surface tension to the air-phase. (σ) (N/m)
air	1.48E-5	1	-
water	1E-6	1000	.07
toluene	6.8E-7	867	.03
DMF	8.5E-7	945	.037
Water/Ethanol (1:3)	2.5E-6	855	.025
DMF/*o*-xylene	9.2E-7	909	

Table S4: Fluid Flow Types.

Liquid Behaviour	Flow transitions
α	Circular → Spicule → Double Helical
β	Spicule only
γ	Double Helical

Table S5: Flow regimes are characterised by the relative length scales of the circular Coriolis (F_c) and Faraday wave (F_{FW}) flows.

Flow Range	Flow transitions
Circular	$F_c > F_{FW}$
Spicule	$F_c \sim F_{FW}$
Double Helical	$F_c < F_{FW}$

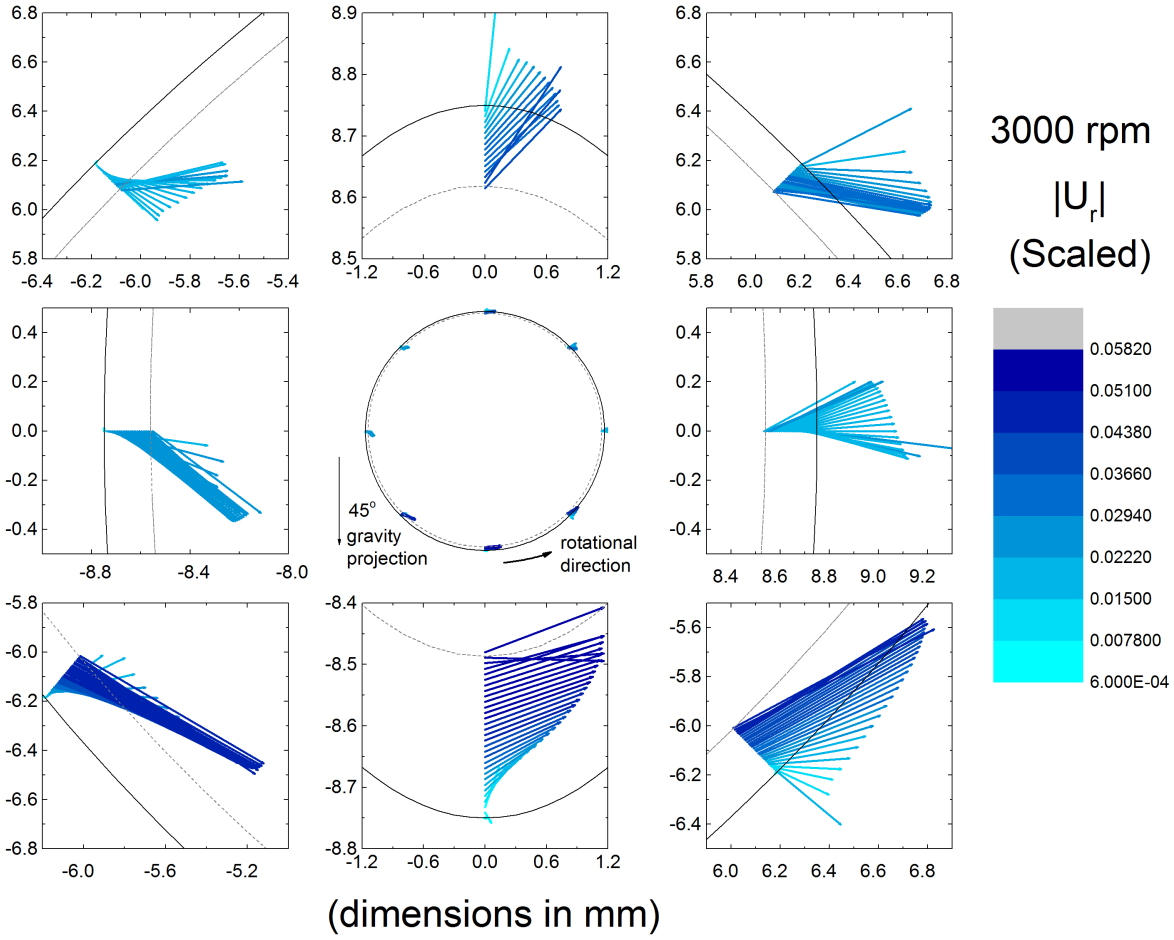

Figure S57: Relative velocity of water across the film thickness at various angular position about the rotational axis of the VFD at a rotational speed of 3000 rpm and a 45° tilt angle. A scale factor of 0.02 has been applied to the relative velocity vector. Solid line- tube wall, grey dashed line – film profile.

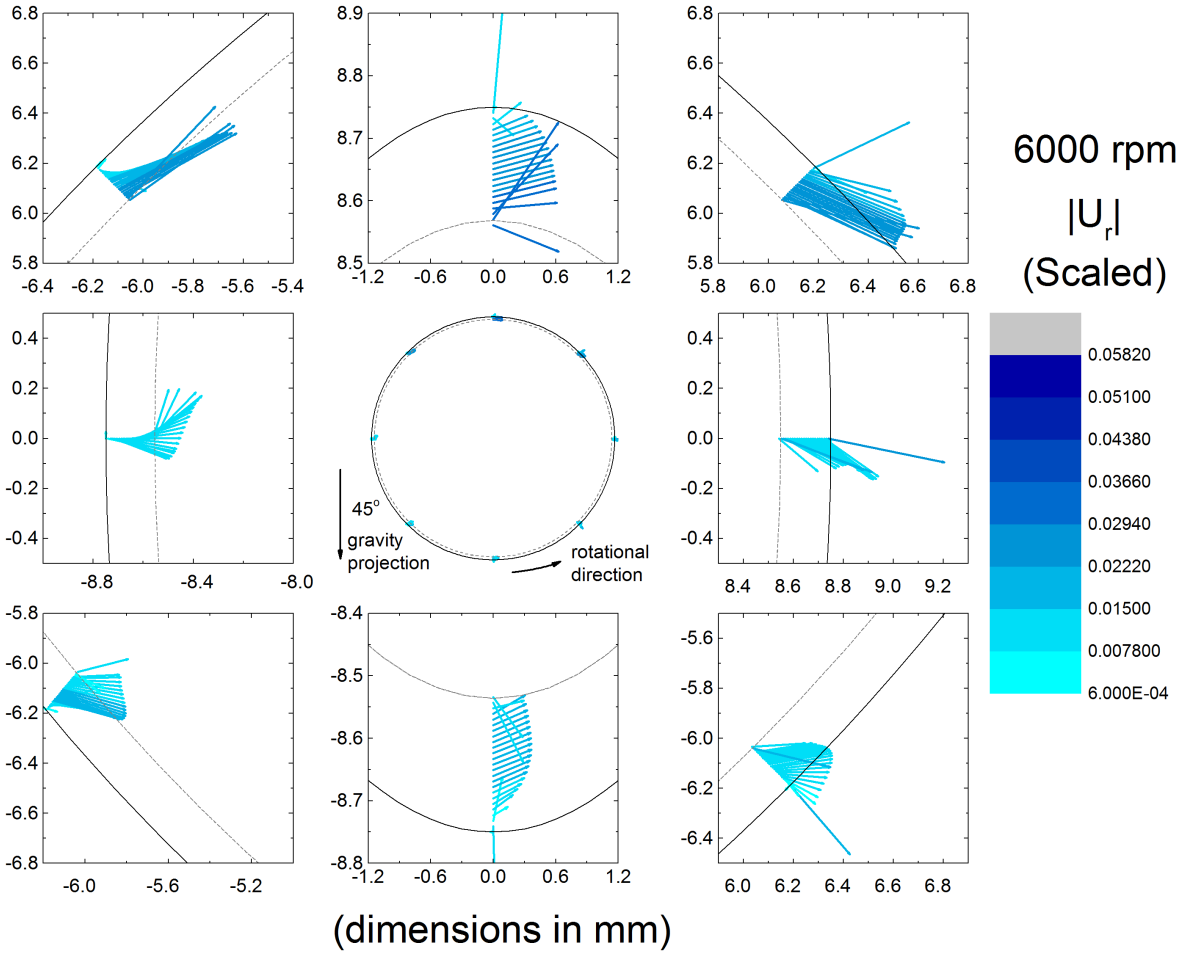

Figure S58: Relative velocity of water across the film thickness at various angular position about the rotational axis of the VFD at a rotational speed of 6000 rpm and a 45° tilt angle. A scale factor of 0.02 has been applied to the relative velocity vector. Solid line- tube wall, grey dashed line – film profile.

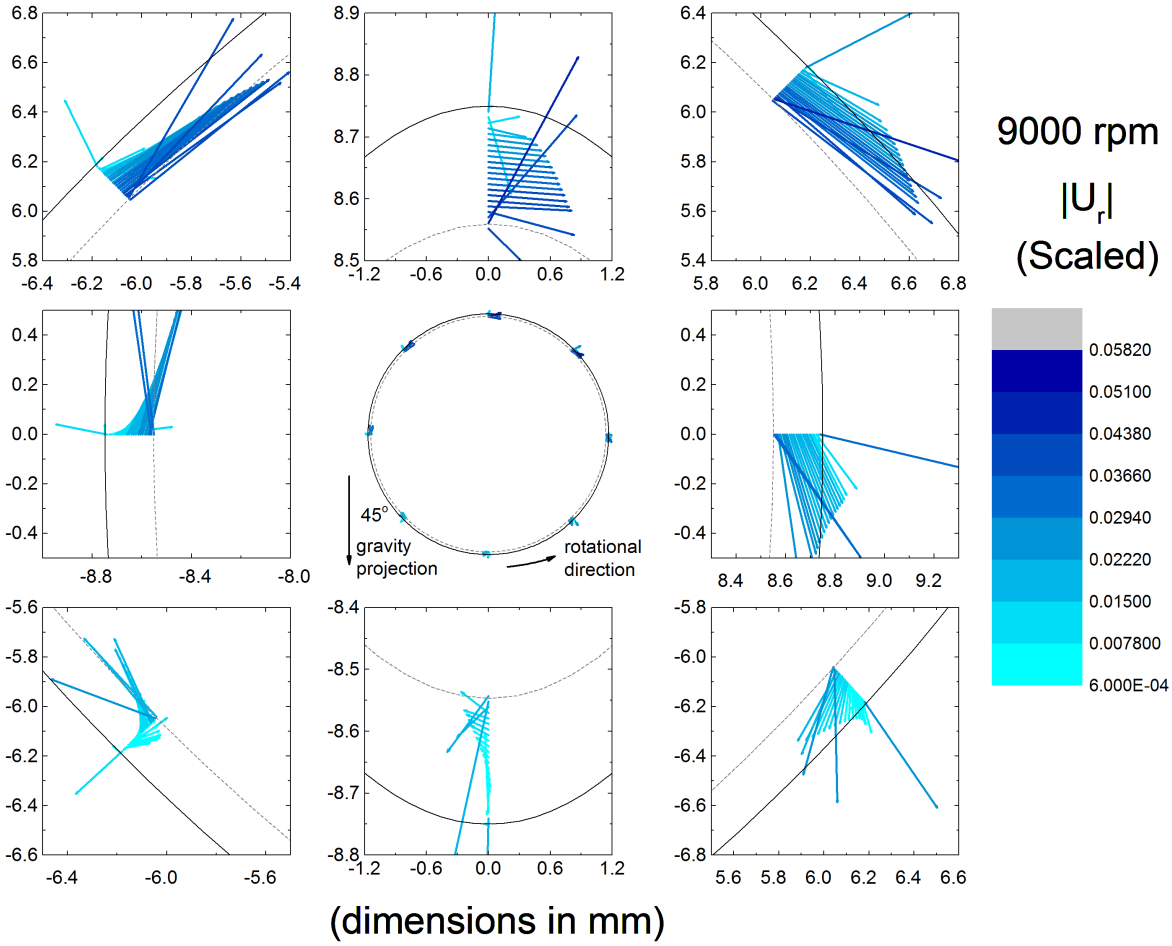

Figure S59: Relative velocity of water across the film thickness at various angular position about the rotational axis of the VFD at a rotational speed of 9000 rpm and a 45° tilt angle. A scale factor of 0.02 has been applied to the relative velocity vector. Solid line- tube wall, grey dashed line – film profile.

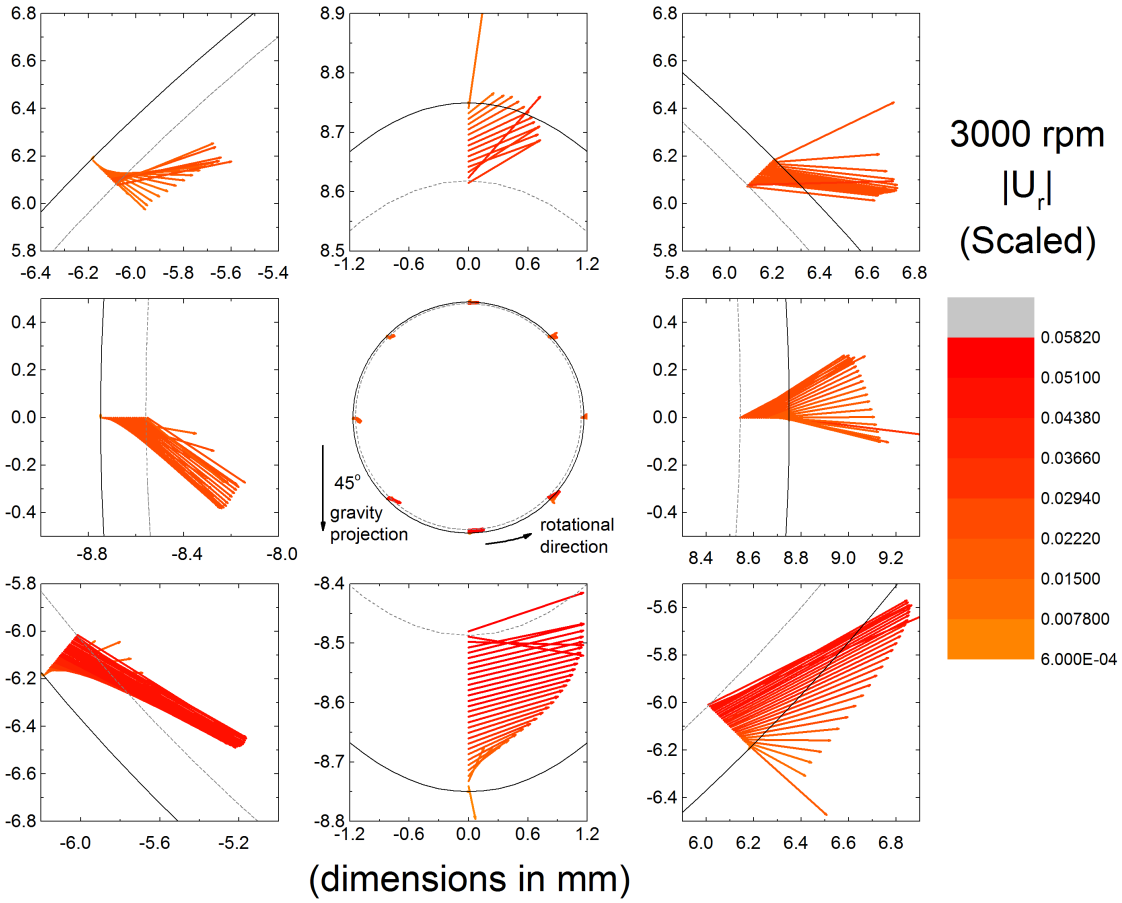

Figure S60: Relative velocity of toluene across the film thickness at various angular position about the rotational axis of the VFD at a rotational speed of 3000 rpm and a 45° tilt angle. A scale factor of 0.02 has been applied to the relative velocity vector. Solid line- tube wall, grey dashed line – film profile.

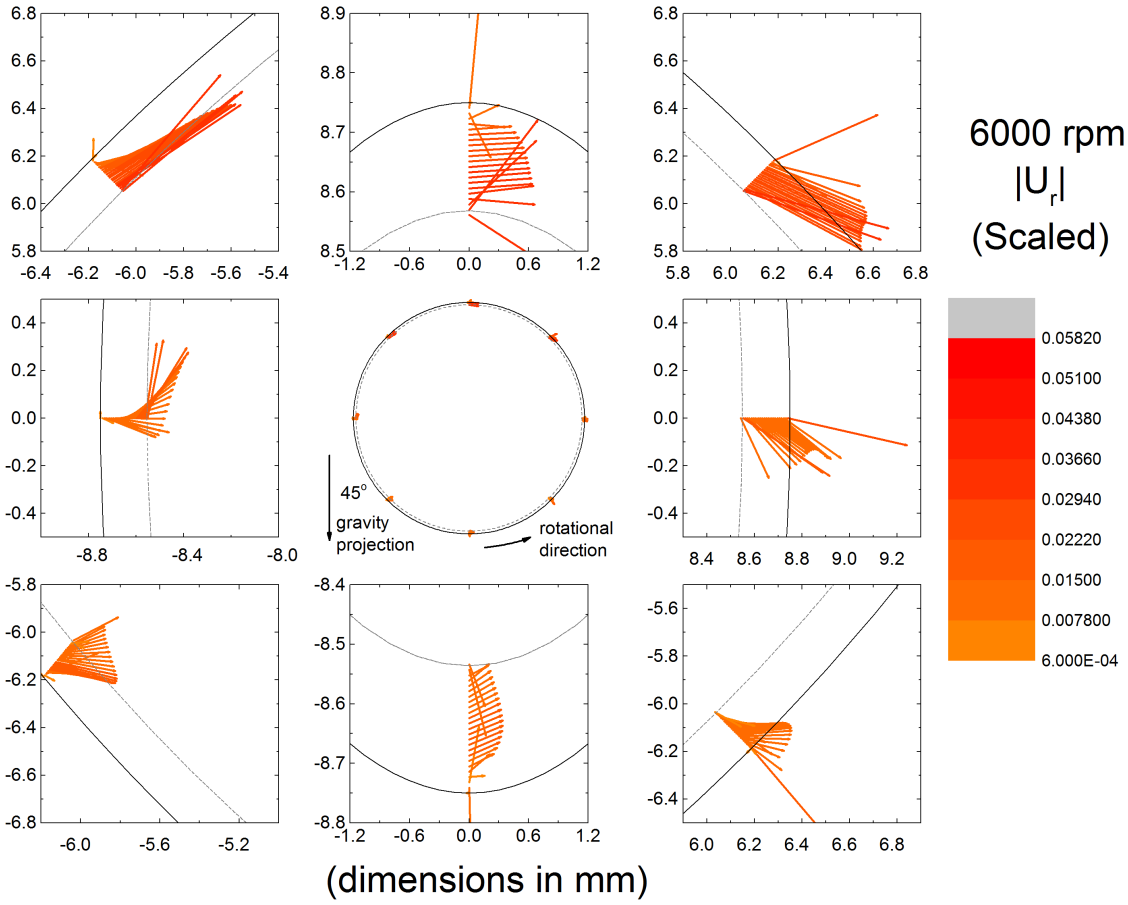

Figure S61: Relative velocity of toluene across the film thickness at various angular position about the rotational axis of the VFD at a rotational speed of 6000 rpm and a 45° tilt angle. A scale factor of 0.02 has been applied to the relative velocity vector. Solid line- tube wall, grey dashed line – film profile.

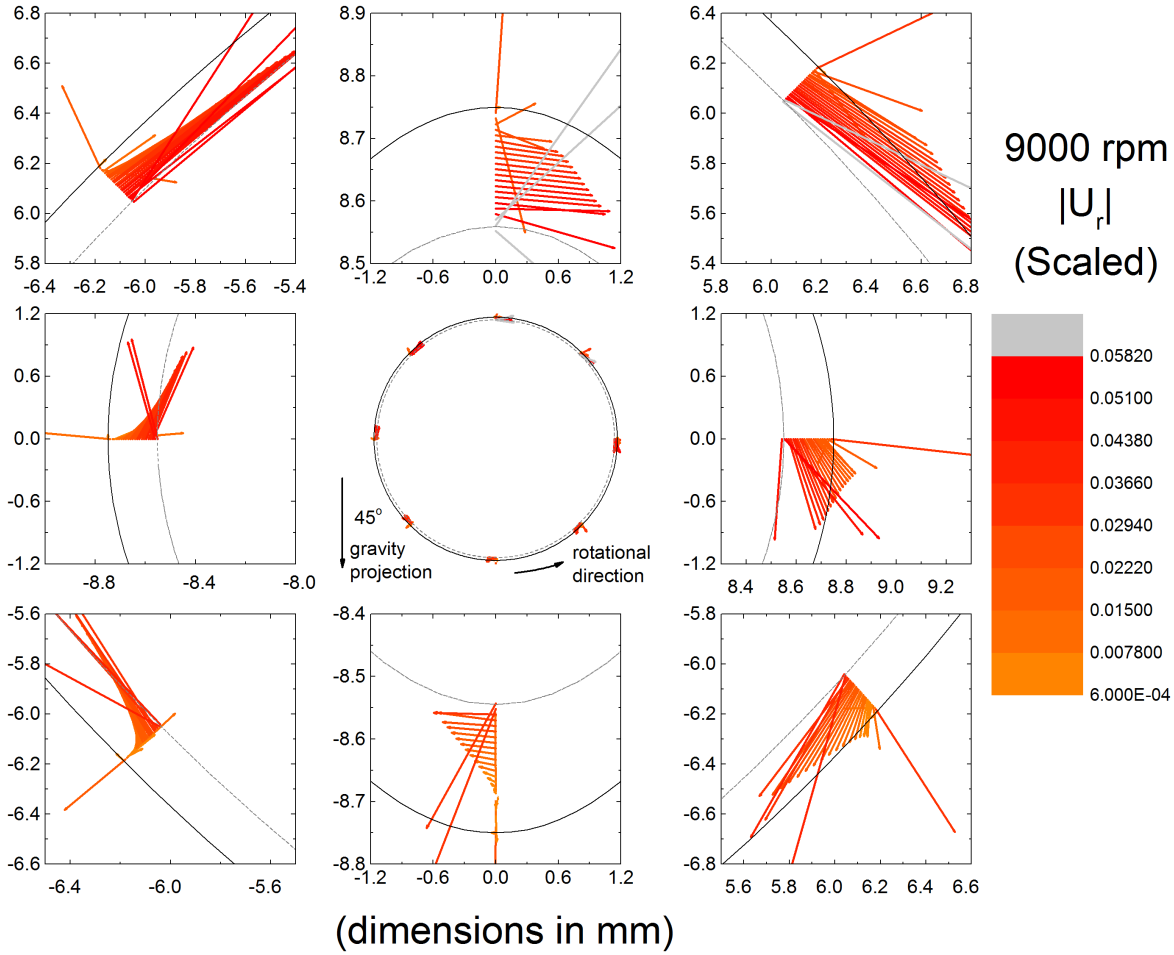

Figure S62: Relative velocity of toluene across the film thickness at various angular position about the rotational axis of the VFD at a rotational speed of 9000 rpm and a 45° tilt angle. Here a scale factor of 0.02 has been applied to the relative velocity vector. Solid line- tube wall, grey dashed line – film profile.

References

1. Alsulami, I. K., Alharbi, T. M. D., Harvey, D. P., Gibson, C. T. & Raston, C. L. Controlling the growth of fullerene C_{60} cones under continuous flow, *Chem. Commun*., **54**, 7896-7899 (2018).
2 Anikina, N.S., Zaginaichenko, S.Y., Maistrenko, M.I., Zolotarenko, A.D., Sivak, G.A., Schur, D.V. and Teslenko, L.O., 2004. Spectrophotometric Analysis of C 60 and C 70 Fullerences in the Toluene Solutions. In *Hydrogen Materials Science and Chemistry of Carbon Nanomaterials* (pp. 207-216). Springer, Dordrecht.
3. Luo, X. et al. Vortex fluidic mediated synthesis of macroporous bovine serum albumin-based microspheres, *ACS Appl. Mater. Interfaces,***10**, 27224−27232 (2018).
4. Stormonth-Darling, J. M., Pedersen, R. H., How, C. & Gadegaard, N. Injection moulding of ultra high apsect ratio nanstrucutres using coated polymer tooling, *J. Micromech. Microeng*., **24**, 075019 (2014).
5. C. Zheng, C., Greer, H. F. Chiang, C.-Y., & Zhou, W. Microstructural study of the formation mechnaism of metal-organic framework MOF-5, *CrystEngComm* **16**, 1064-1070 (2014).
6. Tranchemontagne, D. J., Hunt, J. R. & Yaghi, O. M. Room temperature synthesis of metal-organic frameworks: MOF-5, MOF-74, MOF-177, MOF-199, and MOFOF-0, *Tetrahedron* **64**, 8553-8557 (2008)
7. Millward, A. R., & Yaghi, O. M.Metal-organic frameworks with exceptionally high capacity for storage of carbon dioxide at room temperature, *J. Am. Chem. Soc.* **127**, 17998-17999 (2005).
8. Greathouse, J. A. & Allendorf, M. D. The interaction of water with MOF-5 simulated by molecular mechanics, *J. Am. Chem. Soc,* **128**, 10678-10679 (2006).
9. OpenFOAM v1806, www.openfoam.org (2019).
10. Ng, H. C.-H., Cregan, H. L. F., Dodds, J. M., Poole R. J. & Dennis, D. J. C. Partially filled pipes: experimentas in laminar and tubulent flow, *J. Fluid Mech.* **848**, 467 (2018).